Revisiting the role of cAMP in Drosophila aversive olfactory memory formation

Takashi Abe[1†*], Daisuke Yamazaki[1†], Makoto Hiroi[1,2], Yutaro Ueoka[1], Yuko Maeyama[1] and Tetsuya Tabata[1*]

[1]Institute for Quantitative Biological Sciences, The University of Tokyo, Tokyo, Japan.

[2]Present address Okinawa Institute of Science and Technology.

[†]These authors contributed equally to this work

[*]For Correspondence: tabe@iqb.u-tokyo.ac.jp (TA); ttabata@iqb.u-tokyo.ac.jp (TT)

Abstract

In the olfactory aversive conditioning of Drosophila melanogaster, an odor, the conditioned stimulus (CS), is associated with electric shock, the unconditioned stimulus (US). The Rutabaga adenylyl cyclase in Kenyon cells (KCs) of the fly brain synthesizes cAMP, which is believed to serve as the coincidence detector synergistically stimulated by calcium/calmodulin evoked by the odor reception and GαS released in response to the dopamine signaling elicited by electric shock. However, live imaging analyses revealed that olfactory stimulation itself elicited the activation of dopaminergic neurons and resulted in the elevation of cAMP levels in KCs that received dopamine, regardless of calcium signaling. This finding raises questions about the longstanding and fundamental comprehension of conditioning mechanisms, as the cAMP levels in CS+ KCs could not be distinguished from those in the rest of the KCs. Our data indicate that the cAMP level is an unlikely candidate for serving as a memory engram. Furthermore, our findings demonstrate that cAMP has an adverse impact on the release of acetylcholine from KCs. Accordingly, we postulate that, during conditioning, cAMP depresses KCs, thereby skewing the valence of the CS+ odor towards a more aversive state for the conditioned flies, ultimately culminating in the formation of aversive memories.

Introduction

A quintessential aspect of classical conditioning involves the temporal pairing of an initially neutral stimulus, the conditioned stimulus (CS), with a reinforcing stimulus, the unconditioned stimulus (US), and the preservation of this association at the level of synaptic connections, leading to the manifestation of a conditioned response to the CS (Rescorla, 1988). The temporal correlation between the CS and US is mediated by coincidence detection mechanisms. One of the well-known coincidence detectors is adenylyl cyclase (AC), which is stimulated by both calcium/calmodulin and G-proteins coupled to receptors and catalyzes the conversion of ATP to cAMP. This was first revealed by the pioneering studies on classical conditioning of gill-withdrawal in the sea mollusca Aplysia. When siphon stimulation (CS) and electric shock to the tail (US) were repeatedly paired, CS elicited potentiated gill- and siphon-withdrawal reflexes (Carew et al., 1981). Integration of the calcium influx resulting from CS and the serotonin release resulting from the shock to the tail (US) increased the cAMP levels (Ocorr et al., 1985), as also shown biochemically (Abrams and Kandel, 1988; Yovell et al., 1992). These physiological and biochemical studies highlighted the pivotal role of adenylyl cyclase as a coincidence detector, which was strengthened by the genetic dissection of another model for the classical conditioning of Drosophila olfactory memory (Abrams and Kandel, 1988; Levin et al., 1992; Livingstone et al., 1984; Tully, 1987; Tully and Quinn, 1985). Odor information via acetylcholine (ACh) signaling represents the CS (Gu and O'Dowd, 2006), and G-proteins coupled to dopamine metabotropic receptors (Kim et al., 2007) activated by dopaminergic neurons encode the US (electric shocks or sugar reward) in Drosophila (Burke et al., 2012; Liu et al., 2012; Riemensperger et al., 2005; Schwaerzel et al., 2003). These two input pathways converge on the Rutabaga adenylyl cyclase (AC) (Davis, 1993; Livingstone et al., 1984) expressed in

Kenyon cells (KCs)(McGuire et al., 2003; Zars et al., 2000) of the mushroom bodies (MBs)(Heisenberg, 2003).

Genetically-encoded fluorescent sensors have recently enabled the microscopic visualization of the dynamics of AC activities in fly brains. Tomchik and Davis showed the Rutabaga AC-dependent synergistic increase in cAMP in α/β and α'/β' KCs when acetylcholine (CS) and dopamine (US) application were paired to *ex vivo* brain explants (Tomchik and Davis, 2009). They also demonstrated that elevating cAMP acutely enhanced KC excitability. Additionally, Handler et al. reported a synergistic increase in cAMP levels in γ KCs upon temporal pairing of acetylcholine application with dopamine neuron activation in *ex vivo* brain explants (Handler et al., 2019). Gervasi et al. employed protein kinase A (PKA) activity as an indicator of cAMP levels, and reported that the simultaneous administration of acetylcholine and dopamine led to an augmentation of PKA activity exclusively in α/β KCs, in a manner dependent on Rutabaga AC (Gervasi et al., 2010). These findings collectively indicate that the Rutabaga AC fulfills its long-held role as a coincidence detector. It is worth noting, however, that these imaging experiments did not measure cAMP or PKA transients at a cellular resolution, but rather as a unit of the lobe, comprising a cluster of KC axons. It is estimated that, on average, roughly 20% of KCs exhibit a consistent response to monomolecular odors such as 3-octanol (OCT) and 4-methylcyclohexanol (MCH), as employed in these experiments (Honegger et al., 2011). This sparse nature of coding is essential for distinguishing a conditioned stimulus (CS+) odor from a non-conditioned stimulus (CS-) odor in classical conditioning. Thus, if the Rutabaga AC serves as the coincidence detector, then upon pairing with dopamine input (US), the cAMP levels in the odor-evoked Kenyon cells (CS+) should be notably elevated in comparison to the remaining KCs. Recently, it has been demonstrated that the axo-axonic connections mediated by the muscarinic type-B receptor exert a suppressive

effect on dopamine-evoked cAMP in neighboring KCs, thereby preventing weakly activated and unreliably responding KCs (off-target KCs) from being erroneously classified as the genuine CS+ KCs. This phenomenon of lateral inhibition is deemed essential for memory formation (Manoim et al., 2022). To the best of our knowledge, there is no direct evidence that the cAMP levels in CS+ KCs are higher than those in the remaining KCs following classical conditioning. However, this serves as a crucial indicator of AC functioning as the coincidence detector. Therefore, live imaging should ideally be conducted at a cellular resolution, with the CS and US provided by presenting odors and electric shocks, respectively, to replicate the parsimony of coding and the authenticity of signals. With this objective in mind, we established an imaging system that simultaneously records cAMP and calcium transients in the KCs of head-opened Drosophila melanogaster observed under a two-photon microscope. We verified that odor presentation (CS) evoked not only calcium influx but also dopamine release (Mao and Davis, 2009; Riemensperger et al., 2005) and discovered that it induced robust cAMP increases even in the absence of US, in axons that did not exhibit elevated calcium levels. This substantial cAMP elevation, which is dependent on dopamine signaling but not on calcium concentration, raises questions about the long-established fundamental understanding of conditioning mechanisms. Based on re-evaluations of the CS- or US-evoked cAMP, calcium, and dopamine transients, PKA activity, and acetylcholine (ACh) release in KCs at near single-cell resolution, we discuss what has been overlooked in the Drosophila model of classical conditioning.

Results

Odor presentation evokes cAMP elevation in a broad population of KCs independently of calcium responses

The mushroom bodies (MBs) in the Drosophila brain are the locus of olfactory classical conditioning (Heisenberg, 2003). The ~2,000 Kenyon cells (KCs) of the MBs are classified into three subtypes that extend axons into the α/β, α'/β', and γ lobes (Crittenden et al., 1998)(Figure 1A). These lobes can be subdivided anatomically and functionally into 15 non-overlapping compartments, each innervated by distinct dopamine neuron (DAN) populations (Aso et al., 2014; Tanaka et al., 2008). In Drosophila olfactory conditioning, Rutabaga adenylyl cyclase (Rut AC) is thought to serve as the coincidence detector in KCs (McGuire et al., 2003; Zars et al., 2000)(Figure 1B). Dubnau and his colleagues have shown that Rutabaga AC expression is required in both α/β KCs and γ KCs to support aversive memory fully (Blum et al., 2009), and the dopamine receptor Dop1R1 expression in γ KCs is sufficient to support aversive memory (Qin et al., 2012). In addition, protocerebral posterior lateral 1 (PPL-1) cluster dopamine neurons (DANs) projecting to the γ1, γ2, and α3 compartments and protocerebral anterior medial (PAM) cluster DANs projecting to the γ3 compartment of KCs reinforced negative valence (Aso et al., 2012; Yamagata et al., 2016). Elevations of cAMP levels and protein kinase A (PKA) activity reportedly exhibited a synergistic effect following the pairing of a conditioned stimulus and an unconditioned stimulus in the α lobe in the context of aversive conditioning paradigms (Gervasi et al., 2010; Tomchik and Davis, 2009) and in the γ lobe in the context of appetitive conditioning paradigms (Handler et al., 2019). Thus, we focused on the γ and α lobes in subsequent live imaging experiments (Figure 1C-G). Responses to odors were measured as calcium transients with the genetically encoded fluorescent sensor jRGECO1b (Dana et al., 2016) and cAMP levels were measured with G-Flamp1 (Wang et al., 2022) simultaneously.

The two sensors were initially expressed with the γCRE-p Gal4 (Yamazaki et al., 2018) driver, as it encompasses a smaller subset of γ KCs compared to other γ KC

drivers, enabling the ability to achieve single-cell resolution within a dense neuropile. Specifically, the γCRE-p driver covers approximately 350 (Yamazaki et al., 2018) out of 701 γ KCs (Li et al., 2020). The γ lobe comprises five compartments, with the γ1 compartment being the most distal. Initially, imaging of the γ2-5 compartments was performed to achieve the optimal balance of resolution and scanning speed (Figure 1C). In general, a sequence of images, with a consistent focus, was captured at a frequency of approximately 2 frames per second, while three distinct olfactory stimuli, specifically 3-octanol (OCT), 4-methyl cyclohexanol (MCH), and apple cider vinegar (ACV), each with a duration of 3 seconds, and an electrical shock lasting 10 milliseconds, were successively administered. Prominent calcium responses were observed in a limited number of axons (Figure 1C), reflecting the sparse coding nature of KCs (Honegger et al., 2011). The γ KC axons branch and traverse the lobe in a meandering manner, as depicted schematically in Figure 1A, resulting in single-plane images of calcium responses often appearing interrupted and patchy. As previously reported (Wang et al., 2022), we also detected odor-evoked cAMP signals with the second channel, which varied in a compartment-specific manner along the length of the lobes with distinct characteristics for each odor, and the most robust signal was identified within the γ4 compartment upon MCH or ACV presentation (Figure 1D). Notably, there was no evidence of cAMP being selectively synthesized in odor-responding (as marked by the calcium signals in Figure 1C) axons. A significant elevation in cAMP was observed in a population of axons spanning almost the entire width of a limited number of compartments. In contrast, the calcium signal was detected in a small number of axons but across the entire length of the γ2-5 compartments. These profiles can be described as orthogonal and suggest that cAMP levels are largely independent of calcium concentrations. An electrical stimulus elicits cAMP synthesis in the γ2 compartment, albeit with variable signal strength (Figure 1C).

156 Thus, the fly's behavior should be vigilantly monitored each time the electrical stimulus
157 is administered and the shock responses must be confirmed. Additionally, the split
158 Gal4 driver MB364B, which expresses α/β and γ KCs, was used to eliminate any
159 potential bias in cAMP signaling, as the γCRE-p driver consists of 12 tandem CRE
160 (cAMP responsive element) sequences in the control region (Yamazaki et al., 2018)
161 and may be more likely to drive a population of cells responsive to cAMP signaling.
162 The γ1-5 compartments were similarly subjected to imaging upon exposure to
163 comparable olfactory and electrical stimuli. The calcium and cAMP transient profiles in
164 MB364B-positive γ KCs were virtually congruent with those observed in γCRE-p
165 (Figure 1E). A significant increase in cAMP levels was noted in axons traversing nearly
166 the full breadth of the γ lobe, whereas the calcium signal was only discernible in a
167 limited number of axons. An electrical stimulus elicited cAMP synthesis in the γ1 and
168 γ2 compartments, and in γ3 to a lesser extent. Responses in β lobe were also imaged
169 using the MB364B driver; however, they were not further analyzed. We subsequently
170 used the OK107 driver to visualize the α3 compartment, which was similarly subjected
171 to olfactory stimuli and electrical stimulation. A transverse optical section of the densely
172 packed neuropil in the α3 compartment enabled the observation of all α/β KCs within a
173 single focal plane. This view unequivocally illustrated that cAMP synthesis is subject to
174 compartmental regulation, as indicated by the considerable increase in cAMP levels
175 observed in the majority, if not all, of KCs upon exposure to MCH or OCT, while
176 uniformly minimal responses were detected upon exposure to ACV, regardless of
177 individual KCs' odor-specific responses (Figure 1F-G). In summary, the cAMP levels
178 display odor-specific and compartment-dependent patterns, regardless of calcium
179 levels. Our focus will be on investigating the behavior of γ KCs, as the γ1 and γ2
180 compartments are the sites of short and mid-term aversive memory formation (Aso et
181 al., 2010; Aso and Rubin, 2016).

182 **Dopamine elicits cAMP synthesis**

183 We subsequently inquired whether the dopamine signal modulates the cAMP synthesis
184 elicited by odor stimulus, given that odor-evoked cAMP transients vary among odors
185 and odors activate DANs (Cervantes-Sandoval et al., 2017; Mao and Davis, 2009;
186 Riemensperger et al., 2005; Sun et al., 2020). The widespread dissemination of cAMP
187 within compartments may be attributed to dopamine's release through the process of
188 volume transmission (Liu et al., 2021). We subsequently employed $GRAB_{DA}$ (Sun et al.,
189 2020) to image dopamine and Pink Flamindo (Harada et al., 2017) to visualize cAMP in
190 the γ lobe, to assess the geometric correlation between the two signals. Two instances
191 showing distinct compartment-specific signals were chosen to exemplify the
192 interrelatedness between the two signals (Figure 2A). The results inferred that
193 dopamine and cAMP demonstrate a robust correlation (Figure 2B). However, caution
194 must be exercised when drawing conclusions at the cellular level, given the divergent
195 kinetics between these two sensors and the comparatively lower signal-to-noise ratio of
196 Pink Flamindo in relation to G-Flamp1. To further elucidate the role of dopamine, the
197 cAMP levels were measured in a functionally null mutant of the type I dopamine
198 receptor, Dop1R1 (Akiba et al., 2019), which is coupled with GαS (Sugamori et al.,
199 1995) and thus engaged in activating adenylyl cyclase. The cAMP signals showed
200 substantial attenuation in the Dop1R1 mutant, thereby implying the necessity of the
201 dopamine signal for the activation of adenylyl cyclase (Figure 2C-D). We additionally
202 observed subtle signals within the γ1 compartment following the administration of the
203 shock stimulus, which could potentially be ascribed to the sensitization of adenylate
204 cyclase by Gαi/o-coupled receptors independent of Dop1R1 (Watts and Neve, 2005). It
205 is worth noting that the simultaneously recorded calcium signal was significantly
206 augmented when odors were presented, in comparison to the wild type (Figure 2E).
207 These experiments showed that odor stimulus alone evokes cAMP synthesis by

activating both PPL-1 DANs, which project to the γ1 and γ2 compartments, and PAM (protocerebral anterior medial) DANs, which project to the γ3-5 compartments. PPL-1 DANs also reinforce electric shock and PAM DANs also reinforce sugar reward, the US, implying that the presentation of the odors, CS, is inextricably linked with the presentation of the US.

The correlation between calcium and cAMP levels when odor and shock are paired

As previously noted, the long-held principle of coincidence detection posits that cAMP levels in CS+ KCs should be specifically elevated when the odor stimulus and electric shock are paired. How does this occur, despite the fact that the odor-evoked cAMP rise does not depend on the calcium concentration, but on dopamine released from the same PPL-1 neurons that also reinforce the shock information? To answer this question, we conducted microscopic imaging of calcium and cAMP transients in the γ lobe of head-fixed flies that expressed G-Flamp1 and jRGECO1b driven by the γCRE-p or MB364B GAL4 driver. The flies were subjected to OCT in conjunction with the administration of electric shock, replicating the established paradigm of aversive memory conditioning. Electric shock increased cAMP levels in the γ1-2 compartments (Figure 1), as two sets of PPL-1 DANs, γ1pedc and γ2α'1, are known to convey aversive signals. We examined the cAMP transients specifically in the γ1 and γ2 compartments in an enlarged imaging field. We did not observe a significant cAMP elevation that highlighted CS+ KCs in either case (Figure 3A). In the γ1 compartment of the fly harboring the γCRE-p GAL4 driver, the degree of elevation in response to the simultaneous application of OCT and shock was nearly equivalent to the summation of responses to each stimulus presented independently (Figure 3B). However, in the γ2 compartment, the degree of elevation was even lower than the sum of the responses to

each stimulus applied independently (Figure 3B). These results were not unexpected, as the cAMP levels rely largely on the dopamine release facilitated by the same DANs activated by both CS and US. However, these findings are in stark contrast to previous reports that a synergistic increase, i.e., larger than a simple sum, of cAMP or PKA levels was observed upon association of the two stimuli (Gervasi et al., 2010; Handler et al., 2019; Tomchik and Davis, 2009).

The correlation between calcium and cAMP levels was further evaluated using scatterplots (Figure 3C). We examined representative images. No significant associations were observed between calcium and cAMP levels (γ1: R^2 = 0.0076, γ2: R^2 = 0.0881). It is worth contemplating that roughly ~20% of KCs manifest temporal dynamics that give rise to an elevation in calcium levels (Honegger et al., 2011), while a significant majority of KCs synthesize cAMP in response to dopaminergic stimulation upon exposure to a particular olfactory stimulus. Hence, it is plausible for the calcium and cAMP signals to exhibit some degree of overlap, even in the absence of a causative link between the two signals. On the contrary, assuming the complete dependency of cAMP synthesis on calcium levels, the plot could be simulated in the following manner. The timeline images extracted from the identical bout of calcium imaging employed in Figure 3C were segregated into odd-numbered and even-numbered images, and subjected to a scatterplot analysis against each other, thereby simulating the representation of calcium levels in even-numbered frames as cAMP levels (Figure 3D). This simulation yielded R^2 values of 0.462 (γ1) and 0.756 (γ2). Thus, while we cannot dismiss the possibility that cAMP synthesis may require a specific threshold of calcium, it is irrefutable that the cAMP levels are not entirely contingent upon calcium levels when odor and electric shock are paired. In other words, the cAMP level cannot function as the engram for detecting coincidences between odor and electric shock.

cAMP in aversive conditioning

As described, the cAMP level in each compartment depends on receiving dopamine conveying negative valence (punishment signal like electric shock) to the γ1-3 compartments (Aso et al., 2012; Yamagata et al., 2016) and positive valence (reward signal like sugar digestion) to the γ4-5 compartments (Liu et al., 2012). Moreover, discrete compartments can be identified in relation to odor valence, wherein the DANs projecting to the γ2 compartment connote aversive valence, in contrast to the DANs projecting to the γ4 (Kato et al., 2022; Siju et al., 2020). Furthermore, DANs integrate odor valence and shock signals (Huang et al., 2022). Given the hypothesis that the cAMP level roughly corresponds to the dopamine level and that cAMP acts as an intermediary for dopamine's role in determining odor valence, achieving a state of balanced cAMP levels across the γ lobe could provide a comprehensive representation of integrated valence. This can be visualized as a two-dimensional image displaying cAMP levels across different compartments and is referred to as the cAMP code. We posited that the cAMP code might represent the neural plasticity mechanism engaged in aversive conditioning. Although the absolute cAMP levels exhibited variations among individuals for each odor, we hypothesized that the relative cAMP levels of the γ2 (corresponding to negative valence) and γ4 or γ5 (corresponding to positive valence) compartments, the γ2/4 or γ2/5 cAMP ratio, may constitute a quantitative metric for evaluating the valence of an olfactory stimulus for an individual. As such, any variations in the γ2/4 or γ2/5 cAMP ratio prior to and post-conditioning could be employed to assess the differential response to the stimulus, reflecting the acquisition of memory. To this end, we attempted to replicate aversive conditioning under a microscope by subjecting the fly to three consecutive episodes of electric shocks while exposing it to OCT, followed by exposure to MCH and ACV without electric shocks (OCT as CS+), or exposing it to MCH with electric shocks and to OCT and ACV without electric shocks

286 (MCH as CS+) (Figure 4A). During the process, cAMP transients were recorded for
287 each exposure and quantified (Figure 4B-G). Note that, based on the innate behavioral
288 responses, OCT and MCH are both similarly aversive compared to air, whereas ACV is
289 attractive (Badel et al., 2016). Before conditioning, the medians of the γ2/4 cAMP ratios
290 for the three odors followed the order of OCT>MCH>ACV.

291 The association of OCT with electric shock led to an increase in the relative
292 levels of cAMP in the γ1 and γ2 compartments, primarily attributed to the shock
293 stimulus (Figure 4B). This was followed by a significant elevation in the γ2/4 and γ2/5
294 cAMP ratios of OCT even after the pairing, while no discernible alterations were
295 noticed in MCH or ACV, which were not used in electric shock pairing (Figure 4D and
296 F). Conversely, when MCH was paired with electric shock, there was an increase in the
297 γ2/4 and γ2/5 cAMP ratios of MCH, while no significant alteration was observed in
298 either OCT or ACV (Figure 4E and G). It appears that the cAMP code of odor A is
299 integrated with the cAMP code of electric shock, resulting in the formation of an
300 aversively learned cAMP code for odor A even after the conditioning (Figure 4D and E,
301 CS+ panels).
302

303 **The protein kinase A (PKA) activities coincide with the presence of cAMP**

304 Protein kinase A (PKA) is a prominent subject of cAMP modulation, making it a suitable
305 indicator to probe the functional status of the observed cAMP population. We employed
306 the expression of a protein kinase A (PKA) sensor, ExRai-AKAR2 (Zhang et al., 2021),
307 in combination with Pink Flamindo, to examine whether the PKA activity aligns with the
308 spatial distribution of cAMP. Despite the constraints posed by the signal-to-noise ratios
309 of these sensors, which impeded our comprehensive examination of signals at a
310 cellular level, the dynamics of PKA activities unveiled a profound correlation with the
311 cAMP signal (Figure 5A). This correlation was apparent not only within individual

312 compartments but also manifested as a population code, whereby the profiles of the
313 signal across five compartments collectively responded to a range of olfactory stimuli
314 (Figure 5A-B). These findings suggest that a substantial portion of the cAMP identified
315 in this investigation possesses functional efficacy in activating PKA.
316
317 **cAMP depresses ACh release from KCs**
318 The KCs are recognized as cholinergic (Barnstedt et al., 2016; Yasuyama and
319 Salvaterra, 1999), and their ACh release after aversive conditioning is reportedly
320 attenuated in the γ1 (Zeng et al., 2023), γ2 and γ3 (Stahl et al., 2022; Zeng et al.,
321 2023), and α'3 compartments (Zhang et al., 2019). It has recently been reported that
322 Rutabaga AC decreases ACh release from KCs (Noyes and Davis, 2023). Our findings
323 were in concordance with these observations. We conducted simultaneous imaging of
324 ACh and cAMP transients in the γ KCs of flies expressing the ACh sensor, $GRAB_{ACh\ 3.0}$,
325 and Pink Flamindo, under the control of the MB364B GAL4 driver. Subsequently,
326 aversive conditioning was administered to the flies while they were observed under the
327 microscope (Figure 6A-D). While the ratios of γ2/4 cAMP and γ2/5 cAMP in CS+ OCT
328 also exhibited a notable increase (6C and D, upper left panels) as mentioned above,
329 the ratios of γ2/4 ACh and γ2/5 ACh in CS+ OCT exhibited a notable decrease (6C and
330 D, lower left panels). No such changes were observed in CS- MCH or ACV.
331 We subsequently examined the evoked responses following exposure to three
332 different olfactory stimuli in the Dop1R1 mutant (Figure 7A-B), wherein we observed a
333 notable increase in ACh levels in contrast to the genetic control (Figure 7C), which is
334 incongruent with the prior report showing a reduction in ACh levels in the Dop1R1
335 knockdown condition (Noyes and Davis, 2023). As previously mentioned (Figure 2D),
336 the levels of cyclic cAMP declined (Figure 7B, upper panels). Subsequently, we
337 proceeded to monitor the release of ACh by activating adenylyl cyclase through the

bath application of Forskolin, aiming to investigate whether cAMP, rather than another component downstream of dopamine, attenuates the ACh release (Figure 7D, left). Upon the administration of Forskolin, we observed a remarkable increase in the cAMP levels, concurrent with a reduction in the ACh levels, in the γ2 compartment (Figure 7D, right). This observation signifies the involvement of cAMP in the attenuation of ACh release. This was corroborated through the quantification of signals across five compartments exposed to olfactory stimuli and the subsequent observation of signal recovery following the washout of Forskolin (Figure 7E-F). It is worth noting, however, that the extents of the impacts exerted by Forskolin, the augmentation in cAMP levels and the reduction in ACh release, were decreased in the Dop1R1 mutant (data not shown). These findings align with the previous report indicating the synergistic stimulation of adenylyl cyclases by GαS and Forskolin (Sutkowski et al., 1994).

Discussion

Our study suggests that cAMP levels do not act as the "memory engram" marker for the merging of the conditioned and unconditioned stimuli during memory formation. Instead, cAMP acts as a reinforcer downstream of dopamine, suppressing acetylcholine release from KCs and consequently modulating the DAN-KC-MBON recurrent feedback loop (Adel and Griffith, 2021) in a valence-dependent manner. We hereby propose that the cAMP levels across the γ compartments of the mushroom body can be designated as the "cAMP code", which serves as an indicator of the integrated valence experienced by the individual.

There is no evidence to indicate that cAMP levels serve as a memory engram

Physiological and cellular studies on Aplysia gill withdrawal (Abrams and Kandel, 1988; Ocorr et al., 1985; Yovell et al., 1992) and genetic studies on Drosophila olfactory

364 conditioning (Heisenberg, 2003; Levin et al., 1992; Livingstone et al., 1984; Mons et al.,
365 1999; Tully, 1987; Tully and Quinn, 1985) solidified the idea of adenylyl cyclase as a
366 coincidence detector. This also holds for vertebrates. For example, pre-post pairing
367 (CS) and dopamine (US) signals are thought to converge on adenylyl cyclase in reward
368 learning (reward prediction error) in the striatum (Urakubo et al., 2020; Yagishita et al.,
369 2014).

370 Our research aimed to directly examine this long-standing hypothesis by
371 observing the *in vivo* cAMP and calcium or dopamine transients at near single-cell
372 resolution, which revealed some incongruities. First, the presentation of an odor elicits
373 dopamine release from the same populations of DANs that mediate shock signals, as
374 previously reported (Mao and Davis, 2009; Riemensperger et al., 2005), demonstrating
375 that the CS is invariably coupled with the US, thereby diminishing the synergistic
376 effects. Indeed, the odor presentation alone induces a robust elevation of cAMP levels
377 in KCs, independent of their response to the relevant odor. The anticipated synergy
378 was not detected, as we failed to observe a specific increase in cAMP levels in CS+
379 KCs, even in the γ1 and γ2 compartments, which are indispensable and adequate for
380 the acquisition of short- and middle-term memories (Aso et al., 2012). These results
381 contradict the notion that adenylyl cyclase functions as a coincidence detector (Figure
382 8A).

383 Nevertheless, we cannot formally preclude the possibility that the core site of
384 the Rutabaga action or the coincidence detection was within a microenvironment that
385 we failed to access, or the population of cAMP synthesized with Rutabaga at the
386 coincidence detection was masked by the pool of cAMP synthesized with other
387 adenylyl cyclases. The overlap between the positive PKA signal and that of cAMP
388 suggests that the cAMP signal detected in the current study was sufficiently functional
389 to activate PKA. The following discussion is based on the assumption that the detected

390 cAMP signal is functional. Although our findings indicate that the CS+ KCs cannot be
391 differentiated from the other KCs based on cAMP levels, in essence meaning that
392 cAMP levels do not serve as the "memory engram" marker of the integration of the CS
393 and US during memory acquisition, the cAMP signal still holds significant importance in
394 memory formation. In the realm of mammalian reward learning, the convergence of
395 calcium-mediated NMDAR signaling and dopamine has been demonstrated and
396 modeled to occur on AC (Urakubo et al., 2020; Yagishita et al., 2014). Nair et al. put
397 forth a theoretical framework where the cAMP/PKA signal activated by dopamine
398 converges with the calcium signal at CaMKII when the inputs of calcium and dopamine
399 are delivered in temporal proximity and in a dopamine-following-calcium sequence
400 (Nair et al., 2016). This role of CaMKII could underly the case of Drosophila olfactory
401 conditioning, since CaMKII accumulation in the KC axons is required for Drosophila
402 aversive and appetitive conditioning (Adel et al., 2022; Chen et al., 2022).
403 The Rutabaga AC is not necessarily involved in all phases of aversive
404 olfactory memory. While the Rutabaga AC is crucial for labile anesthesia-sensitive
405 memory (ASM), it is dispensable for anesthesia-resistant memory (ARM). On the other
406 hand, the Dunce phosphodiesterase 4 is essential for ARM, yet non-essential for ASM,
407 despite both Rutabaga and Dunce serving in the cAMP pathway (Scheunemann et al.,
408 2012). Additionally, the presence of Rutabaga is concurrently required within both α/β
409 and γ KCs, whereas Dunce operates in both KCs and antennal lobe local neurons
410 (Scheunemann et al., 2012). Another olfactory memory paradigm, known as "trace
411 conditioning," does not require the Rutabaga AC and allows the presentation of the
412 conditioned stimulus (CS) and the unconditioned stimulus (US) to be temporally
413 separated by intervals of up to 60 s (Shuai et al., 2011). The Rutabaga AC has been
414 identified as the sole type-I AC in Drosophila (Livingstone, 1985), and its activation by
415 calcium and the GαS subunit has led to its postulation as a coincidence detector for the

416 CS and US. This implies that the underlying mechanism for the convergence of ARM
417 and trace conditioning relies on another AC or an alternative mechanism.
418
419 **Another model for coincidence detection**
420 Various findings have called into question the prevailing notion that AC integrates both
421 calcium and dopamine signals. Saitoe et al. proposed that AC mediates the integration
422 of odor input and the aversive input of electric shocks conveyed by glutamate, but not
423 dopamine; rather, dopamine release is elicited subsequent to this pairing event and
424 serves solely as a reinforcement, but not the US (Saitoe, 2021; Ueno et al., 2017).
425 Recently, Qiao et al. demonstrated that the PPL1 DANs modulate the input-timing-
426 dependent plasticity of γ KC synapses from projection neurons, depending on type 2
427 dopamine receptor (DD2R) (Qiao et al., 2022). Their findings further indicated that the
428 activation of the PPL1-DD2R pathway elicits a rise in calcium levels, which is
429 dependent on the voltage-gated calcium channel (VGCC). They concluded that the
430 VGCC could serve as the coincidence detector. However, this conclusion does not
431 extend to all phases of aversive memory, as the authors also demonstrated that DD2R
432 is not necessary for short-term memory formation.
433 The potential role of the DAN-KC-MBON recurrent feedback loop in the
434 formation of olfactory memory raises the prospect that the synaptic connections
435 between KCs and MBONs may also rely on spike-timing-dependent plasticity (STDP)
436 (Zeng et al., 2023). Between KCs and MBONs in locusts, Cassenaer and Laurent have
437 shown that pre-post pairing causing STDP can, when accompanied by the local
438 administration of a reinforcement-modulating neuromodulator such as dopamine
439 (three-factor neo-Hebbian learning rule), designate the synapses subject to an
440 associative alteration (Cassenaer and Laurent, 2012). This is likely to apply to
441 Drosophila as well. It is noteworthy that comprehensive anatomical studies have

disclosed direct dopaminergic connections from DANs to MBONs in Drosophila α/β KCs (Takemura et al., 2017). Pribbenow et al. have indeed demonstrated that concurrent dopamine release and focal acetylcholine application to the dendrites of the M6 (MBON-γ5β'2a), circumventing KC activity, induce plasticity in calcium transients within this MBON (Pribbenow et al., 2022). Zeng et al. further found that the dorsal paired medial (DPM) neuron releases 5-HT on KCs and regulates the coincidence time window, which has been hypothesized by several theories to be a timing regulator (Zeng et al., 2023). Consequently, we postulate that cAMP is not implicated in coincidence detection, which could depend on the neo-Hebbian learning rule, whereas cAMP functions as a reinforcer downstream of dopamine, as elaborated below.

The dopamine population activities serve as the substrate for the storage of aversive olfactory memory

Upon exposure to different odors, distinct populations of DANs exhibit specific activity patterns, as documented in multiple studies (Berry et al., 2012; Huang et al., 2022; Kato et al., 2022; Mao and Davis, 2009; Yamagata et al., 2016). This, in turn, generates the cAMP code in the γ lobe, which is approximately antithetical to the level of ACh release (Figure 8B). Given that the sustained population dynamics among DANs, likely facilitated by the dynamic interactions within the DAN-KC-MBON recurrent feedback loop, integrate changes in physiological states and environmental cues (Huang et al., 2022; Kato et al., 2022; Siju et al., 2020), the formation of associative memories could be an integral component of this dynamism. This is consistent with the additional finding that repeated exposure to an aversive odor can give rise to a labile, self-reinforced aversive memory for that odor (Jacob et al., 2021). This suggests that the mere presentation of the odor can modulate cAMP levels, which can ultimately lead to outcomes similar to those observed in conditioning with an electric shock. If the odor

and electric shock stimuli are expressed as the cAMP code, then it can be posited that the electric shock serves as an extreme manifestation of the odor stimuli (Figure 8C), since both olfactory stimuli (CS) and electric shock (US) activate overlapping populations of DANs. Thus, in this particular memory paradigm, there appears to be no significant distinction between the odor CS and the electric shock US. Assuming this to be true, the inquiry into the location and mechanism of memorization for the learned population activities of DANs could be comparable to the question of where and how odor-specific population activities of DANs, in general, are retained.

In addition to the well-established function of exogenously activated γ1-pedc DAN as the aversive US (Aso et al., 2012; Aso and Rubin, 2016), the suppression of the corresponding MBON, γ1-pedc>α/β, can also serve as an aversive US (König et al., 2019; Ueoka et al., 2017), as noted (Yamada et al., 2023). These discoveries suggest that not only the stimulation of the γ1pedc DAN, but also the inhibition of γ1pedc>α/β MBON can trigger a series of events that tilt the population activities of DANs towards the aversively learned state. Assuming that the population activities of DANs are consistently revised by the DAN-KC-MBON recurrent feedback loop that integrates inputs from relevant compartments, alterations in the γ1 compartment triggered by augmented γ1 DAN activity or decreased γ1 MBON activity could potentially trigger a complete rewrite of the population activities of DANs.

Recently, the postsynaptic plasticity traces associated with nicotinic acetylcholine receptors in MBONs were reported to contribute to memory storage in appetitive memory (Pribbenow et al., 2022), although their involvement in aversive memory is yet to be established. The underlying cause of this plasticity can be attributed to the previously described neo-Hebbian learning rule. However, it remains unclear how this plasticity leads to changes in the population activities of DANs, resulting in alterations in the shape of the cAMP code. Based on these assumptions,

494 we propose the following model for the formation of aversive olfactory memories. Upon
495 exposure to odor A paired with an electric shock, the release of ACh from the γ1 and
496 γ2 compartments of responsive KCs is attenuated because of the increase in cAMP
497 levels, leading to a depression of the γ1 and γ2 MBONs. This subsequently triggers the
498 reorganization of the dopamine population activities, as well as the reorganization of
499 ACh receptors within the γ1 and γ2 MBON synapses. Consequently, the cAMP code
500 for odor A is shifted towards a more negative valence in comparison to its pre-
501 conditioning state (Figure 8C). The cAMP pathway exerts inhibitory control over ACh
502 release in accordance with the population activities of DANs. Despite the current lack
503 of knowledge regarding the higher-order mechanisms responsible for the organization
504 of the DAN-KC-MBON recurrent feedback loop (Figure 8B), recent progress in
505 unraveling the hierarchical architecture of the DAN circuit (Yamada et al., 2023) holds
506 promise for illuminating these mechanisms in the near future.
507

508 **Materials and methods**

509 **Fly strains**

510 Fly strains were maintained on standard food containing cornmeal at 25°C. The
511 following strains were used. CRE-p65-AD/CyO; MB247-Gal4-DBD (Yamazaki, 2018),
512 UAS-G-Flamp1 attp40/CyO and UAS-G-Flamp1 VK00005 (gifts from Jun Chu and
513 Yulong Li, Nat. Commun., 2022.13:5363), UAS-jRGECO1b VK00005 (#BL63795),
514 MB364B-Gal4 i.e., R13F02-p65-AD attp40; R21B06-Gal4-DBD attP2 (#BL68318),
515 OK107-gal4 (#Ktoto DGRC 106098), UAS-Pink Flamindo su(Hw) attP5 and UAS-Pink
516 Flamindo VK00027 (this study), UAS-GRAB_DA2m attp40 (BL#90878), Dop1R1^{KO}
517 (D1R1 KO, a gift from Taro Ueno, Eur. J. Neurosci. 2020;51:822–839), UAS-ExRai-
518 AKAR2 VK00005 (this study), and UAS-GRAB_ACh3.0 attp40 (BL#86549).
519

520 **Fly genotypes used by figures**

Figure	Genotype
1C, 1D, 2E, 3A, 3B, 3C, 3D	CRE-p65-AD, UAS-G-Flamp1 attp40 / UAS-G-Flamp1 attp40; MB247-GAL4-DBD, UAS- jRGECO1b VK00005 / UAS-jRGECO1b VK00005
1E, 3A, 4B, 4C, 4D, 4E, 4F, 4G	R13F02-p65-AD attp40/ UAS-G-Flamp1 attp40; R21B06-GAL4-DBD attP2, UAS- jRGECO1b VK00005 / +
1F, 1G	UAS-G-Flamp1 attp40 / +; UAS- jRGECO1b VK00005 / + ; OK107-Gal4 / +
2A, 2B	CRE-p65-AD, UAS-GRAB_DA2m attp40, UAS-Pink Flamindo su(Hw)attp5 / UAS-GRAB_DA2m attp40, UAS-Pink Flamindo su(Hw)attp5; UAS-Pink Flamindo VK00027 / +
2C, 2D, 2E	CRE-p65-AD, UAS-G-Flamp1 attp40 / UAS-G-Flamp1 attp40; MB247-GAL4-DBD, UAS- jRGECO1b VK00005, Dop1R1[KO] / UAS- jRGECO1b VK00005, Dop1R1[KO]
5A, 5B	R13F02-p65-AD attp40 / UAS-Pink Flamindo su(Hw)attp5; R21B06-GAL4-DBD attP2 / UAS-ExRai-AKAR2 VK00005
6A, 6B, 6C, 7C, 7D, 7E, 7F	R13F02-p65-AD attp40, UAS-Pink Flamindo su(Hw)attp5 / UAS-GRAB_ACh3.0; R21B06-GAL4-DBD attP2 / +
7A, 7B, 7C	R13F02-p65-AD attp40, UAS-Pink Flamindo su(Hw)attp5 / UAS-GRAB_ACh3.0; R21B06-GAL4-DBD attP2, Dop1R1[KO] / Dop1R1[KO]

521

522 **Construction of UAS-Pink Flamindo and UAS-ExRai-AKAR2**

523 The Pink Flamindo cDNA was amplified by PCR from the plasmid (provided by

524 Kitaguchi, Addgene plasmid #102356). The amplified fragment was then integrated into

525 the 20xUAS vector originating from pJFRC7-20xUAS-IVS-mCD8::GFP (Pfeiffer,
526 Addgene plasmid #26220) by In-Fusion recombinase (Clontech Laboratories). The
527 ExRai-AKAR2 cDNA codon was optimized for Drosophila melanogaster (Eurofins
528 Genomics), and the resulting synthesized cDNA was cloned into the 20xUAS vector
529 described above.
530
531 **Live imaging**
532 **Chemicals**
533 Saline (103 mM NaCl, 3 mM KCl, 10 mM trehalose, 10 mM D-glucose, 26 mM
534 $NaHCO_3$, 1 mM NaH_2PO_4, 1.5 mM $CaCl_2$_$2H_2O$, 4 mM $MgCl_2$_$6H_2O$, 9 mM sucrose,
535 and 5 mM HEPES, (osmolarity adjusted to 270–280 mol/kg), Mineral oil (Fisher
536 Scientific, Fair Lawn, NJ, USA, Cat# O1214), 4-methylcyclohexanol, MCH (Cat#
537 66360, 98%>purity, Fluka, Sigma-Aldrich, St. Louis, MO, USA), 3-octanol, OCT (Cat#
538 74870, 95%>purity, Fluka, Sigma-Aldrich, St. Louis, MO, USA), Apple cider vinegar,
539 ACV (Mizkan jun-ringo-su, Mizkan holdings, Japan, ASIN#B000H2SCTW), Forskolin,
540 Fsk (Tokyo Chemical Industry, Cat# F0855), and Ethanol (Fujifilm Wako, Japan, Cat#
541 054-00466).
542
543 **Fly preparation**
544 Unless otherwise specified, female flies aged 5-16 days were used. A fly was mounted
545 on a custom-made imaging dish immediately after anesthetization by CO_2 gas spray for
546 3–5 s. The head capsule and dorsal thorax were secured to the dish by light-curing
547 glue (DYMAX Medical Adhesive, 1204-M-SC, USA). The proboscis was also glued
548 onto the capsule to reduce brain movement. A window on the top of the head capsule
549 was opened using sharp forceps (Corte Instruments, USA) and a thin injection needle

550 in saline. Air sacs and fat bodies were carefully removed, and muscle 16 was cut using
551 forceps to avoid excessive brain movements during imaging.
552
553 **Olfactory stimulation**
554 Odors were delivered with a custom-made, 8-channel olfactometer controlled by a
555 custom LabVIEW application (National Instruments). While a fly was mounted under
556 the microscope, a constant stream of pure air (0.4 L/min) was directed at the fly. Thirty
557 mL of odor solution was placed in a 100 ml glass bottle (Duran, Cat# TGK 371-05-20-
558 03) with an Omnifit GL45 bottle cap (Diba Omnifit, Cat# OM4212), PTFE tube (Cat#
559 BLS181033, ⅛" x 2.4mm), and USL-PTFE joint (OOU-095-7x1/8", custom-made, 7mm
560 x ⅛", http//www.u-s-l.co.jp). All odorants except for ACV were diluted 1 : 10 vol/vol in
561 mineral oil. ACV was diluted 1 : 10 vol/vol in Milli-Q water. After a stimulation trigger, a
562 solenoid valve redirects a portion of the air stream through the headspace of the glass
563 bottle for 3 s. Two mass flow controllers (SEC-E40, HORIBA STEC, Japan) were used
564 in parallel to regulate the flow of pure air and odors. The odor stream rejoined the pure
565 air stream 40 cm from the end of the odor delivery tube (4 mm in diameter). The odor
566 was released from a position 5 mm in front of the fly at a flow rate of 0.4 L/min.
567 Subsequently, it was collected through a tube (3 mm in diameter) located 15 mm
568 behind the fly at a flow rate of 2 L/min using a vacuum pump (ULVAC DA-20D, ULVAC
569 KIKO, Inc.) equipped with a charcoal filter. The intervals between odor exposures were
570 at least 60 seconds.
571
572 **Electric shock delivery**
573 A fly was subjected to electric stimulation by positioning one end of a platinum wire at
574 the base of its legs and the other end at the abdominal region, using a
575 micromanipulator (MNM-25, Narishige, Tokyo, Japan). At the time point 17.5 seconds

576 from the commencement of the recording, a 60-volt electric shock generated with an
577 Electric Stimulator (SEN-3401, Nihon Kohden, Japan) and Isolator (SS-203J, Nihon
578 Kohden, Japan) was administered to the fly for a duration of 10 milliseconds. In the
579 context of pairing odor and electric shock, electric stimulation was applied after a delay
580 of 1.5 seconds following the initiation of a 3-second odor presentation. The
581 administration of the shock was verified by observing the movements of the legs and
582 the occurrence of abdominal cramps using a CCD camera (STC-TB33USB, Omron
583 Sentech, Tokyo, Japan).
584
585 **Forskolin bath application**
586 Forskolin, a compound of interest, was dissolved in a solution containing Saline and
587 100% EtOH in a 3:1 ratio, to make a stock solution with a 5 mM Forskolin
588 concentration. From this stock solution, a working solution was prepared by dilution
589 with Saline to achieve a concentration of 100 μM Forskolin in Saline with 0.5% EtOH.
590 As a control, Saline with 0.5% EtOH was used. For live imaging, the standard Saline
591 solution was removed, leaving a small remaining volume of 50 μl on the objective and
592 dish. Then, a syringe containing Saline with 0.5% EtOH was connected to the dish,
593 allowing the space between the objective and dish to be filled. The recording was
594 performed for a duration of 4 minutes. Subsequently, the Saline with 0.5% EtOH was
595 replaced with 1 mL of the 100 μM Forskolin solution in Saline with 0.5% EtOH, and
596 another 4-minute recording was conducted. During this time, the responses to odors
597 were recorded. At the end of the recordings, the 100 μM Forskolin solution in Saline
598 with 0.5% EtOH was washed out by replacing it with the standard saline solution four
599 times, and the responses to odors under the wash-out conditions were also recorded.
600
601 **Two-photon laser microscopy**

602 For *in vivo* two-photon imaging, we employed a two-photon microscope (Olympus
603 FVMPE-RS; Olympus, Tokyo, Japan) equipped with a water-immersion objective lens
604 (XLPLN25XWM, 25x N.A. 1.05), a titanium:sapphire pulsed laser (INSIGHT DS DUAL-
605 OL; Spectra-Physics, Santa Clara, CA, USA), and a Galvano Scanner to facilitate live
606 imaging. The emitted light was collected using GaAsP photomultiplier detectors with
607 495-540 nm and 575-645 nm bandpass filters (FV30-FGR). G-CaMP6f and G-Flamp1
608 were excited at 925 nm, GRAB_DA2m, GRAB_ACh3.0, and ExRai-AKAR2 were
609 excited at 980 nm, while jRGECO1b and Pink Flamindo were excited at 1040 nm.
610 Using the Olympus FV31S-SW imaging software, we acquired time series images with
611 different dimensions: 400-430 x 130-120 pixels (0.14-0.19 μm/pixel, γ1-γ2 zoom in
612 Figure 3), 275-320 x 155-140 (0.33-0.50 μm/pixel, γ1-γ5 in Figures 1, 2, 4, 5, 6, and 7),
613 and 180-250 x 150-165 (0.15-0.20 μm/pixel, α'3/α3 in Figure 1). The acquisition was
614 performed at a frame rate of either 333 or 500 ms/frame in a sequential line scan
615 mode, ensuring that the time difference between acquiring images for channels 1 and 2
616 was less than 2 ms. By default, images were acquired for a duration of 40 s to capture
617 the response to each stimulus and were saved for subsequent image processing. The
618 solenoid valve for odor stimulation was activated 15 s after the start of each recording,
619 and delivered the odor for a duration of 3 s, corresponding to frames #46-54 (333
620 ms/frame) or #31-36 (500 ms/frame). For quantitative analysis, ΔF/F0 images of peak
621 responses were generated by averaging frames #51-65 (333 ms/frame) or frames #35-
622 44 (500 ms/frame). The experimental flies, which were housed in vials with food, were
623 transferred to an imaging room maintained at a temperature of 22 °C at least two days
624 prior to the imaging experiments.
625
626 **Image analysis**
627 The image analysis was conducted as described previously (Hiroi et al., 2013), with

several modifications. The images within each recording were stabilized using the template matching plugin of Fiji (ImageJ). To mitigate the impact of detector noise and uncorrected movement, all reporter signals underwent an initial processing step employing a median filter (with a radius of 1 pixel). For the images obtained from the same fly, after stabilization, a template matching technique was utilized for alignment. Subsequently, the ΔF values were computed based on the average (F0) of the one-second interval following the opening of the valve (specifically, 15 seconds after the start of the recording). It is important to note that the median filter (with a radius of 1 pixel) was once again applied during this stage. To identify the KC region (also known as the region of interest, ROI), Li's binarizing algorithm was applied to the averaged signal intensity across the entire duration of each recording, using Fiji. Regions of interest (ROIs) for each compartment were first manually identified, using the anatomical characteristics as a guide. The demarcation between the γ3 and γ4 compartments was occasionally challenging to determine, and it was pragmatically established that the border lies within the middle of the regions assigned to the γ3 and γ4 compartments. The drawing and preservation of ROIs, as well as the measurement of ΔF/F0, were performed in a semi-automated manner using both built-in and custom-written macro routines in Fiji. Furthermore, a series of additional image processing tasks, such as correlation testing and temporal dynamics plotting, were executed using MATLAB scripts.

Scatter Plot Analysis

We computed the mean ΔF/F0 values of calcium and cAMP transients within the designated γ1 and γ2 compartments for each pixel during the 1 to 6 seconds following the delivery of OCT or OCT + electrical shock, employing the identical method outlined in the preceding image analysis section. These calculated values were then plotted on

a scatter plot, with calcium represented on the X-axis and cAMP on the Y-axis for each pixel. To assess the linearity of the relationship, we conducted a linear regression analysis on the scatter plot and determined the R^2 value. To simulate the potential maximum linearity between the two values in our experimental setup, we created an additional scatter plot. We divided the dataset obtained from calcium transients into two groups, based on whether the frame number was odd or even. Then, we plotted the values from the odd-numbered frames on the X-axis and the values from the even-numbered frames on the Y-axis. The processes of acquiring data, generating scatter plots, applying linear regression analysis, and calculating R^2 values were all executed utilizing the MATLAB software.

Statistics

Statistical analyses were conducted using the Prism 9 software (GraphPad). All tests were non-parametric, two-tailed, and the confidence levels were set at $\alpha = 0.05$. The figure legends provide the p values and specify the comparisons made for each experiment, unless otherwise indicated. The bar graphs display the means ± SEM for the data.

Acknowledgements

We thank Joshua Johansen, Hokto Kazama, Satoshi Kida, Tom Kornberg, Minoru Saitoe, and Kazumichi Shimizu for their valuable comments. We are grateful to Atsushi Miyajima for providing access to the Ti:sapphire laser. We also thank H. Takishita and M. Sato for excellent help with fly husbandry. We would also like to thank the Kyoto DGRC, the NIG Stock Center, the Bloomington Stock Center, and the Janelia Research Campus/HHMI for fly stocks. This work was supported by grants from the Ministry of Education, Culture, Sports, Science and Technology (17K17681 and

19K16254 to T.A., 21K06388 to D.Y. and 19H03268 to T.T., A.T. and D.Y.) and the Takeda Science Foundation to T.T.

Author contributions: T.A., D.Y. and T.T. designed the research; T.A. performed live imaging and statistical analyses; D.Y. constructed transgenes and performed live imaging in the early phase; M.H. developed an imaging data acquisition system; Y.M. conducted genetic and histological experiments; Y.U. performed statistical analyses. T.A., D.Y. and T.T. wrote the manuscript.

References

Abrams TW, Kandel ER. 1988. Is contiguity detection in classical conditioning a system or a cellular property? Learning in Aplysia suggests a possible molecular site. *Trends Neurosci* 11:128–135. doi:10.1016/0166-2236(88)90137-3

Adel M, Chen N, Zhang Y, Reed ML, Quasney C, Griffith LC. 2022. Pairing-dependent plasticity in a dissected fly brain is input-specific and requires synaptic CaMKII enrichment and nighttime sleep. *J Neurosci* JN-RM-0144-22. doi:10.1523/jneurosci.0144-22.2022

Adel M, Griffith LC. 2021. The Role of Dopamine in Associative Learning in Drosophila: An Updated Unified Model. *Neurosci Bull* 37:831–852. doi:10.1007/s12264-021-00665-0

Akiba M, Sugimoto K, Aoki R, Murakami R, Miyashita T, Hashimoto R, Hiranuma A, Yamauchi J, Ueno T, Morimoto T. 2020. Dopamine modulates the optomotor response to unreliable visual stimuli in Drosophila melanogaster. *Eur J Neurosci* 51:822–839. doi:10.1111/ejn.14648

Aso Y, Hattori D, Yu Y, Johnston RM, Iyer NA, Ngo T-T, Dionne H, Abbott L, Axel R, Tanimoto H, Rubin GM. 2014. The neuronal architecture of the mushroom body provides a logic for associative learning. *eLife* 3:e04577. doi:10.7554/elife.04577

Aso Y, Herb A, Ogueta M, Siwanowicz I, Templier T, Friedrich AB, Ito K, Scholz H, Tanimoto H. 2012. Three dopamine pathways induce aversive odor memories with different stability. *PLoS genetics* 8:e1002768. doi:10.1371/journal.pgen.1002768

Aso Y, Rubin GM. 2016. Dopaminergic neurons write and update memories with cell-type-specific rules. *eLife* 5:e16135. doi:10.7554/elife.16135

Aso Y, Siwanowicz I, Bräcker L, Ito K, Kitamoto T, Tanimoto H. 2010. Specific Dopaminergic Neurons for the Formation of Labile Aversive Memory. *Curr Biol* 20:1445–1451. doi:10.1016/j.cub.2010.06.048

Barnstedt O, Owald D, Felsenberg J, Brain R, Moszynski J-P, Talbot CB, Perrat PN, Waddell S. 2016. Memory-Relevant Mushroom Body Output Synapses Are Cholinergic. *Neuron* 0:1237–1247. doi:10.1016/j.neuron.2016.02.015

Berry JA, Cervantes-Sandoval I, Nicholas EP, Davis RL. 2012. Dopamine is required for learning and forgetting in Drosophila. *Neuron* 74:530–542. doi:10.1016/j.neuron.2012.04.007

Bilz F, Geurten BRH, Hancock CE, Widmann A, Fiala A. 2020. Visualization of a Distributed Synaptic Memory Code in the Drosophila Brain. *Neuron*. doi:10.1016/j.neuron.2020.03.010

Burke CJ, Huetteroth W, Owald D, Perisse E, Krashes MJ, Das G, Gohl D, Silies M, Certel S, Waddell S. 2012. Layered reward signalling through octopamine and dopamine in Drosophila. *Nature* 492:433–437. doi:10.1038/nature11614

Carew T, Walters E, Kandel E. 1981. Classical conditioning in a simple withdrawal reflex in Aplysia californica. *J Neurosci* 1:1426–1437. doi:10.1523/jneurosci.01-12-01426.1981

Cassenaer S, Laurent G. 2012. Conditional modulation of spike-timing-dependent plasticity for olfactory learning. *Nature* 482:47–52. doi:10.1038/nature10776

Cervantes-Sandoval I, Phan A, Chakraborty M, Davis RL, Vijayraghavan K. 2017. Reciprocal synapses between mushroom body and dopamine neurons form a positive feedback loop required for learning. *eLife* 6:e23789. doi:10.7554/elife.23789

Chen N, Zhang Y, Adel M, Kuklin EA, Reed ML, Mardovin JD, Bakthavachalu B, VijayRaghavan K, Ramaswami M, Griffith LC. 2022. Local translation provides the asymmetric distribution of CaMKII required for associative memory formation. *Curr Biol*. doi:10.1016/j.cub.2022.04.047

Crittenden JR, Skoulakis EMC, Han K-A, Kalderon D, Davis RL. 1998. Tripartite Mushroom Body Architecture Revealed by Antigenic Markers. *Learn Memory* 5:38–51. doi:10.1101/lm.5.1.38

Dana H, Mohar B, Sun Y, Narayan S, Gordus A, Hasseman JP, Tsegaye G, Holt GT, Hu A, Walpita D, Patel R, Macklin JJ, Bargmann CI, Ahrens MB, Schreiter ER, Jayaraman V, Looger LL, Svoboda K, Kim DS. 2016. Sensitive red protein calcium indicators for imaging neural activity. *Elife* 5:e12727. doi:10.7554/elife.12727

Davis RL. 1993. Mushroom bodies and drosophila learning. *Neuron* 11:1–14. doi:10.1016/0896-6273(93)90266-t

733 Gervasi N, Tchénio P, Preat T. 2010. PKA dynamics in a Drosophila learning center:
734 coincidence detection by rutabaga adenylyl cyclase and spatial regulation by dunce
735 phosphodiesterase. *Neuron* 65:516–529. doi:10.1016/j.neuron.2010.01.014

736 Gu H, O'Dowd DK. 2006. Cholinergic synaptic transmission in adult Drosophila Kenyon
737 cells in situ. *The Journal of neuroscience : the official journal of the Society for*
738 *Neuroscience* 26:265–272. doi:10.1523/jneurosci.4109-05.2006

739 Handler A, Graham TGW, Cohn R, Morantte I, Siliciano AF, Zeng J, Li Y, Ruta V. 2019.
740 Distinct Dopamine Receptor Pathways Underlie the Temporal Sensitivity of
741 Associative Learning. *Cell* 178:60–75. doi:10.1016/j.cell.2019.05.040

742 Harada K, Ito M, Wang X, Tanaka M, Wongso D, Konno A, Hirai H, Hirase H, Tsuboi T,
743 Kitaguchi T. 2017. Red fluorescent protein-based cAMP indicator applicable to
744 optogenetics and in vivo imaging. *Sci Rep-uk* 7:7351. doi:10.1038/s41598-017-
745 07820-6

746 Heisenberg M. 2003. Mushroom body memoir: from maps to models. *Nature reviews*
747 *Neuroscience* 4:266–275. doi:10.1038/nrn1074

748 Hige T, Aso Y, Rubin GM, Turner GC. 2015. Plasticity-driven individualization of
749 olfactory coding in mushroom body output neurons. *Nature* 526:258–262.
750 doi:10.1038/nature15396

751 Hiroi M, Ohkura M, Nakai J, Masuda N, Hashimoto K, Inoue K, Fiala A, Tabata T.
752 2013. Principal component analysis of odor coding at the level of third-order
753 olfactory neurons in Drosophila. *Genes to cells : devoted to molecular & cellular*
754 *mechanisms*. doi:10.1111/gtc.12094

755 Honegger KS, Campbell RAA, Turner GC. 2011. Cellular-resolution population imaging
756 reveals robust sparse coding in the Drosophila mushroom body. *The Journal of*
757 *neuroscience* 31:11772–11785. doi:10.1523/jneurosci.1099-11.2011

758 Huang C, Luo J, Woo SJ, Roitman L, Li J, Pieribone V, Kannan M, Vasan G, Schnitzer
759 M. 2022. Dopamine signals integrate innate and learnt valences to regulate memory
760 dynamics. *Research Square*. doi:10.21203/rs.3.rs-1915648/v1

761 Jacob PF, Vargas-Gutierrez P, Okray Z, Vietti-Michelina S, Felsenberg J, Waddell S.
762 2021. Prior experience conditionally inhibits the expression of new learning in
763 Drosophila. *Curr Biol* 31:3490–3503. doi:10.1016/j.cub.2021.05.056

764 Kanellopoulos AK, Semelidou O, Kotini AG, Anezaki M, Skoulakis EMC. 2012.
765 Learning and Memory Deficits Consequent to Reduction of the Fragile X Mental
766 Retardation Protein Result from Metabotropic Glutamate Receptor-Mediated
767 Inhibition of cAMP Signaling in Drosophila. *J Neurosci* 32:13111–13124.
768 doi:10.1523/jneurosci.1347-12.2012

769 Kato A, Ohta K, Okanoya K, Kazama H. 2022. Dopaminergic neurons dynamically
770 update sensory values during navigation. *Biorxiv* 2022.08.17.504092.
771 doi:10.1101/2022.08.17.504092

Kim Y-C, Lee H-G, Han K-A. 2007. D1 dopamine receptor dDA1 is required in the mushroom body neurons for aversive and appetitive learning in Drosophila. *The Journal of neuroscience : the official journal of the Society for Neuroscience* 27:7640–7647. doi:10.1523/jneurosci.1167-07.2007

König C, Khalili A, Niewalda T, Gao S, Gerber B. 2019. An optogenetic analogue of second-order reinforcement in Drosophila. *Biol Letters* 15:20190084. doi:10.1098/rsbl.2019.0084

Levin LR, Han PL, Hwang PM, Feinstein PG, Davis RL, Reed RR. 1992. The Drosophila learning and memory gene rutabaga encodes a Ca2+/Calmodulin-responsive adenylyl cyclase. *Cell* 68:479–489.

Li F, Lindsey JW, Marin EC, Otto N, Dreher M, Dempsey G, Stark I, Bates AS, Pleijzier MW, Schlegel P, Nern A, Takemura S-Y, Eckstein N, Yang T, Francis A, Braun A, Parekh R, Costa M, Scheffer LK, Aso Y, Jefferis GS, Abbott LF, Litwin-Kumar A, Waddell S, Rubin GM. 2020. The connectome of the adult Drosophila mushroom body provides insights into function. *eLife* 9. doi:10.7554/elife.62576

Liu C, Goel P, Kaeser PS. 2021. Spatial and temporal scales of dopamine transmission. *Nat Rev Neurosci* 22:345–358. doi:10.1038/s41583-021-00455-7

Liu C, Plaçais P-Y, Yamagata N, Pfeiffer BD, Aso Y, Friedrich AB, Siwanowicz I, Rubin GM, Preat T, Tanimoto H. 2012. A subset of dopamine neurons signals reward for odour memory in Drosophila. *Nature* 488:512–516. doi:10.1038/nature11304

Livingstone MS. 1985. Genetic dissection of Drosophila adenylate cyclase. *Proc National Acad Sci* 82:5992–5996. doi:10.1073/pnas.82.17.5992

Livingstone MS, Sziber PP, Quinn WG. 1984. Loss of calcium/calmodulin responsiveness in adenylate cyclase of rutabaga, a Drosophila learning mutant. *Cell* 37:205–215. doi:10.1016/0092-8674(84)90316-7

Manoim JE, Davidson D, Weiss S, Hige T, Parnas M. 2022. Lateral Axonal Modulation Is Required for Stimulus-Specific Olfactory Conditioning in Drosophila. *Ssrn Electron J*. doi:10.2139/ssrn.4120768

Mao Z, Davis RL. 2009. Eight different types of dopaminergic neurons innervate the Drosophila mushroom body neuropil: anatomical and physiological heterogeneity. *Frontiers in neural circuits* 3:5. doi:10.3389/neuro.04.005.2009

McGuire SE, Le PT, Osborn AJ, Matsumoto K, Davis RL. 2003. Spatiotemporal rescue of memory dysfunction in Drosophila. *Science (New York, NY)* 302:1765–1768. doi:10.1126/science.1089035

Mons N, Guillou JL, Jaffard R. 1999. The role of Ca 2+ /calmodulin-stimulable adenylyl cyclases as molecular coincidence detectors in memory formation. *Cellular and Molecular Life Sciences (CMLS)* 55:525–533. doi:10.1007/s000180050311

809 Nair AG, Bhalla US, Kotaleski JH. 2016. Role of DARPP-32 and ARPP-21 in the
810 Emergence of Temporal Constraints on Striatal Calcium and Dopamine Integration.
811 *Plos Comput Biol* 12:e1005080. doi:10.1371/journal.pcbi.1005080

812 Noyes NC, Davis RL. 2023. Innate and learned odor-guided behaviors utilize distinct
813 molecular signaling pathways in a shared dopaminergic circuit. *Cell Reports*
814 42:112026. doi:10.1016/j.celrep.2023.112026

815 Ocorr KA, Walters ET, Byrne JH. 1985. Associative conditioning analog selectively
816 increases cAMP levels of tail sensory neurons in Aplysia. *Proc National Acad Sci*
817 82:2548–2552. doi:10.1073/pnas.82.8.2548

818 Pribbenow C, Chen Y, Heim M-M, Laber D, Reubold S, Reynolds E, Balles I, Alquicira
819 TFV, Suárez-Grimalt R, Scheunemann L, Rauch C, Matkovic T, Rösner J, Lichtner
820 G, Jagannathan SR, Owald D. 2022. Postsynaptic plasticity of cholinergic synapses
821 underlies the induction and expression of appetitive and familiarity memories in
822 Drosophila. *Elife* 11:e80445. doi:10.7554/elife.80445

823 Qiao J, Yang S, Geng H, Yung W-H, Ke Y. 2022. Input-timing-dependent plasticity at
824 incoming synapses of the mushroom body facilitates olfactory learning in
825 Drosophila. *Curr Biol*. doi:10.1016/j.cub.2022.09.054

826 Qin H, Cressy M, Li W, Coravos JS, Izzi SA, Dubnau J. 2012. Gamma Neurons
827 Mediate Dopaminergic Input during Aversive Olfactory Memory Formation in
828 Drosophila. *Current biology* 22:1–7. doi:10.1016/j.cub.2012.02.014

829 Rescorla RA. 1988. Behavioral Studies of Pavlovian Conditioning. *Annu Rev Neurosci*
830 11:329–352. doi:10.1146/annurev.ne.11.030188.001553

831 Riemensperger T, Völler T, Stock P, Buchner E, Fiala A. 2005. Punishment prediction
832 by dopaminergic neurons in Drosophila. *Current biology* 15:1953–1960.
833 doi:10.1016/j.cub.2005.09.042

834 Saitoe. 2021. A non-canonical on-demand dopaminergic transmission underlying
835 olfactory aversive learning. *Neurosci Res* 178:1–9.
836 doi:10.1016/j.neures.2021.12.008

837 Scheunemann L, Jost E, Richlitzki A, Day JP, Sebastian S, Thum AS, Efetova M,
838 Davies S-A, Schwärzel M. 2012. Consolidated and Labile Odor Memory Are
839 Separately Encoded within the Drosophila Brain. *The Journal of neuroscience : the*
840 *official journal of the Society for Neuroscience* 32:17163–17171.
841 doi:10.1523/jneurosci.3286-12.2012

842 Schwaerzel M, Monastirioti M, Scholz H, Friggi-Grelin F, Birman S, Heisenberg M.
843 2003. Dopamine and octopamine differentiate between aversive and appetitive
844 olfactory memories in Drosophila. *The Journal of neuroscience : the official journal*
845 *of the Society for Neuroscience* 23:10495–10502.

846 Shuai Y, Hu Y, Qin H, Campbell RAA, Zhong Y. 2011. Distinct molecular
847 underpinnings of Drosophila olfactory trace conditioning. *Proceedings of the*

National Academy of Sciences of the United States of America. doi:10.1073/pnas.1107489109

Siju KP, Stih V, Aimon S, Gjorgjieva J, Portugues R, Kadow ICG. 2020. Valence and State-Dependent Population Coding in Dopaminergic Neurons in the Fly Mushroom Body. *Current Biology* 30:2104-2115.e4. doi:10.1016/j.cub.2020.04.037

Stahl A, Noyes NC, Boto T, Botero V, Broyles CN, Jing M, Zeng J, King LB, Li Y, Davis RL, Tomchik SM. 2022. Associative learning drives longitudinally-graded presynaptic plasticity of neurotransmitter release along axonal compartments. *Elife* 11. doi:10.7554/elife.76712

Sugamori KS, Demchyshyn LL, McConkey F, Forte MA, Niznik HB. 1995. A primordial dopamine D1-like adenylyl cyclase-linked receptor from Drosophila melanogaster displaying poor affinity for benzazepines. *Febs Lett* 362:131–138. doi:10.1016/0014-5793(95)00224-w

Sun F, Zhou J, Dai B, Qian T, Zeng J, Li X, Zhuo Y, Zhang Y, Wang Y, Qian C, Tan K, Feng J, Dong H, Lin D, Cui G, Li Y. 2020. Next-generation GRAB sensors for monitoring dopaminergic activity in vivo. *Nat Methods* 17:1156–1166. doi:10.1038/s41592-020-00981-9

Sutkowski EM, Tang W-J, Broome CW, Robbins JD, Seamon KB. 1994. Regulation of forskolin interactions with type I, II, V, and VI adenylyl cyclases by Gs.alpha. *Biochemistry* 33:12852–12859. doi:10.1021/bi00209a017

Sweeney ST, Broadie K, Keane J, Niemann H, O'Kane CJ. 1995. Targeted expression of tetanus toxin light chain in Drosophila specifically eliminates synaptic transmission and causes behavioral defects. *Neuron* 14:341–351. doi:10.1016/0896-6273(95)90290-2

Tanaka NK, Tanimoto H, Ito K. 2008. Neuronal assemblies of the Drosophila mushroom body. *The Journal of comparative neurology* 508:711–755. doi:10.1002/cne.21692

Tomchik SM, Davis RL. 2009. Dynamics of learning-related cAMP signaling and stimulus integration in the Drosophila olfactory pathway. *Neuron* 64:510–521. doi:10.1016/j.neuron.2009.09.029

Tully T. 1987. Drosophila learning and memory revisited. *Trends Neurosci* 10:330–335. doi:10.1016/0166-2236(87)90090-7

Tully T, Quinn WG. 1985. Classical conditioning and retention in normal and mutantDrosophila melanogaster. *J Comp Physiology* 157:263–277. doi:10.1007/bf01350033

Ueno K, Suzuki E, Naganos S, Ofusa K, Horiuchi J, Saitoe M. 2017. Coincident postsynaptic activity gates presynaptic dopamine release to induce plasticity in Drosophila mushroom bodies. *eLife* 6:156. doi:10.7554/elife.21076

886 Ueoka Y, Hiroi M, Abe T, Tabata T. 2017. Suppression of a single pair of mushroom
887 body output neurons in Drosophila triggers aversive associations. *FEBS open bio*
888 7:562–576. doi:10.1002/2211-5463.12203

889 Urakubo H, Yagishita S, Kasai H, Ishii S. 2020. Signaling models for dopamine-
890 dependent temporal contiguity in striatal synaptic plasticity. *PloS computational*
891 *biology* 16:e1008078-24. doi:10.1371/journal.pcbi.1008078

892 Wang L, Wu C, Peng W, Zhou Z, Zeng J, Li X, Yang Y, Yu S, Zou Y, Huang M, Liu C,
893 Chen Y, Li Yi, Ti P, Liu W, Gao Y, Zheng W, Zhong H, Gao S, Lu Z, Ren P-G, Ng
894 HL, He J, Chen S, Xu M, Li Yulong, Chu J. 2022. A high-performance genetically
895 encoded fluorescent indicator for in vivo cAMP imaging. *Nat Commun* 13:5363.
896 doi:10.1038/s41467-022-32994-7

897 Watts VJ, Neve KA. 2005. Sensitization of adenylate cyclase by Gαi/o-coupled
898 receptors. *Pharmacol Therapeut* 106:405–421.
899 doi:10.1016/j.pharmthera.2004.12.005

900 Yagishita S, Hayashi-Takagi A, Ellis-Davies GCR, Urakubo H, Ishii S, Kasai H. 2014. A
901 critical time window for dopamine actions on the structural plasticity of dendritic
902 spines. *Science (New York, NY)* 345:1616–1620. doi:10.1126/science.1255514

903 Yamada D, Bushey D, Li F, Hibbard KL, Sammons M, Funke J, Litwin-Kumar A, Hige
904 T, Aso Y. 2023. Hierarchical architecture of dopaminergic circuits enables second-
905 order conditioning in Drosophila. *Elife* 12. doi:10.7554/elife.79042

906 Yamagata N, Hiroi M, Kondo S, Abe A, Tanimoto H. 2016. Suppression of Dopamine
907 Neurons Mediates Reward 14:e1002586. doi:10.1371/journal.pbio.1002586

908 Yamazaki D, Hiroi M, Abe T, Shimizu K, Minami-Ohtsubo M, Maeyama Y, Horiuchi J,
909 Tabata T. 2018. Two Parallel Pathways Assign Opposing Odor Valences during
910 Drosophila Memory Formation. *Cell reports* 22:2346–2358.
911 doi:10.1016/j.celrep.2018.02.012

912 Yasuyama K, Salvaterra PM. 1999. Localization of choline acetyltransferase-
913 expressing neurons in Drosophila nervous system. *Microsc Res Tech* 45:65–79.
914 doi:10.1002/(sici)1097-0029(19990415)45:2<65::aid-jemt2>3.0.co;2-0

915 Yovell Y, Kandel ER, Dudai Y, Abrams TW. 1992. A Quantitative Study of the
916 Ca2+/Calmodulin Sensitivity of Adenylyl Cyclase in Aplysia, Drosophila, and Rat. *J*
917 *Neurochem* 59:1736–1744. doi:10.1111/j.1471-4159.1992.tb11005.x

918 Zars T, Fischer M, Schulz R, Heisenberg M. 2000. Localization of a Short-Term
919 Memory in Drosophila. *Science (New York, NY)* 288:672–675.
920 doi:10.1126/science.288.5466.672

921 Zeng J, Li X, Zhang R, Lv M, Wang Y, Tan K, Xia X, Wan J, Jing M, Zhang X, Li Yu,
922 Yang Y, Wang L, Chu J, Li Yan, Li Yulong. 2023. Local 5-HT signaling bi-
923 directionally regulates the coincidence time window for associative learning.
924 *Neuron*. doi:10.1016/j.neuron.2022.12.034

Zhang J-F, Liu B, Hong I, Mo A, Roth RH, Tenner B, Lin W, Zhang JZ, Molina RS, Drobizhev M, Hughes TE, Tian L, Huganir RL, Mehta S, Zhang J. 2021. An ultrasensitive biosensor for high-resolution kinase activity imaging in awake mice. *Nat Chem Biol* 17:39–46. doi:10.1038/s41589-020-00660-y

Zhang X, Noyes NC, Zeng J, Li Y, Davis RL. 2019. Aversive Training Induces Both Presynaptic and Postsynaptic Suppression in Drosophila. *Journal of Neuroscience* 39:9164–9172. doi:10.1523/jneurosci.1420-19.2019

Competing interest

The authors declare that no competing interests exist.

935 **Figures**

Figure 1

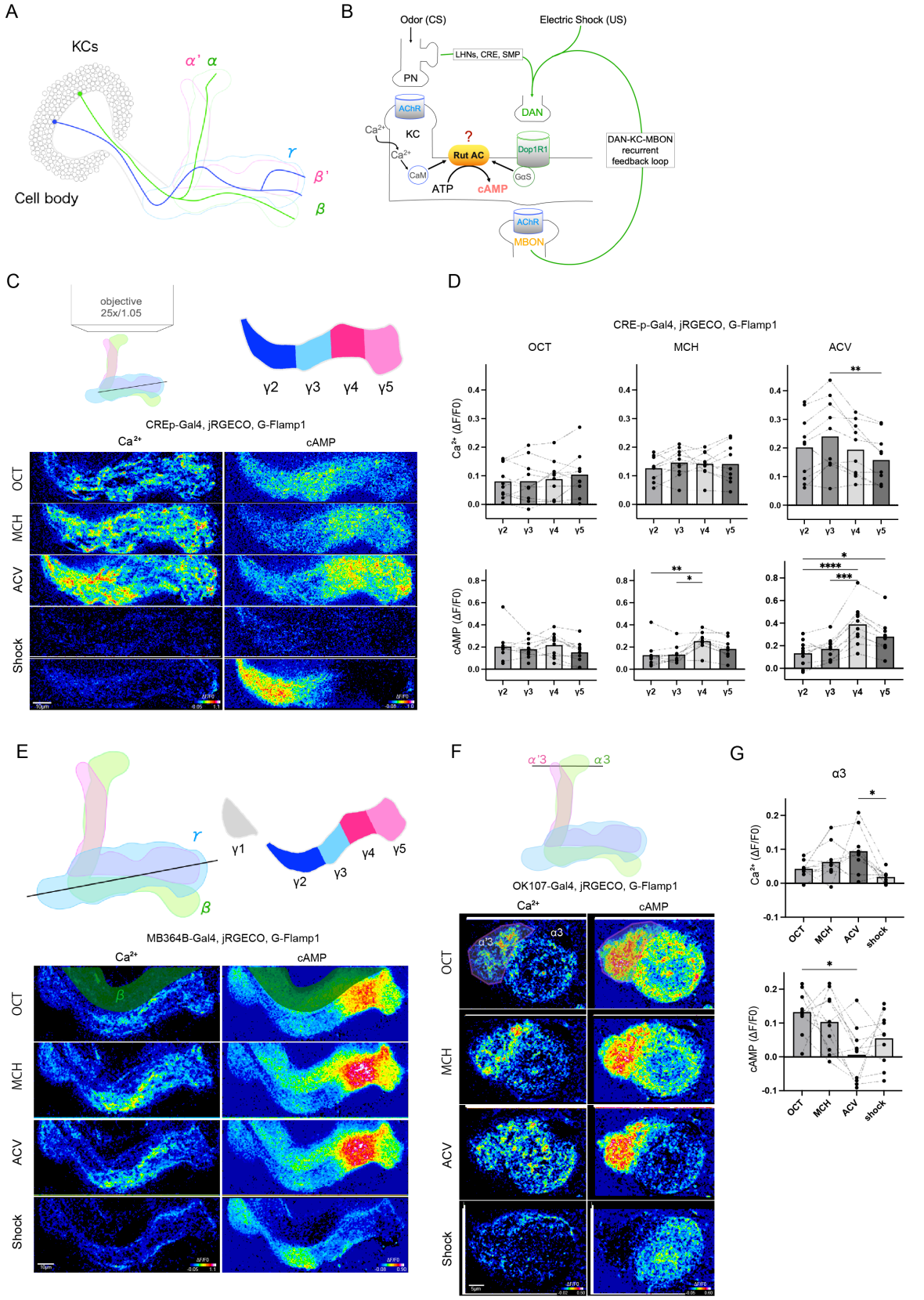

936 **Figure 1.** Odor presentation alone increases dopamine and cAMP in γ KCs. (A)
937 Schematic of Kenyon cells (KCs), referred to Figure 1A (Bilz et al., 2020). The cell
938 body, the α/β, α'/β' and γ lobes, and α/β and γ KCs are depicted. (**B**) Schematic of the
939 role of the Rutabaga adenylyl cyclase (Rut AC) as the coincidence detector. KCs
940 innervated by PPL-1 DANs. The odor acquisition (CS) activates acetylcholine signaling
941 and elevates calcium concentrations through voltage-gated calcium channels. PPL1
942 DANs integrate odor information and noxious stimuli (US) such as electric shock
943 through regions including the lateral horns (LHNs), Crepine (CRE), and superior medial
944 protocerebrum (SMP)(Kato et al., 2022). DANs activities are also regulated by the
945 DAN-KC-MBON recurrent feedback loop (Adel and Griffith, 2021). The CS and US
946 pathways can converge on the Rut AC, which is synergistically activated by the
947 calcium/calmodulin complex and Gα subunit of the G-protein complex coupled to the
948 D1-like dopamine receptor Dop1R1. (**C**) Schematic representation of *in vivo* imaging of
949 KCs. The objective and frontal view of the KCs along with the focal plane (upper left),
950 and the dorsal view of γ KCs with color-coded γ2-5 compartments (upper right) are
951 shown. Exemplary, finely resolved pseudocolor images of averaged peak responses
952 (10 frames for 5 s) of calcium and cAMP during the presentations of 4-
953 methylcyclohexanol (MCH), 3-octanol (OCT), apple cider vinegar (ACV), and electric

954 shock (Shock, two bouts) in γ2-γ5 KCs of the fly expressing G-Flamp1 and jRGECO1b
955 driven by the γCRE-p-Gal4 driver. All images in the present study were acquired using
956 a dual-channel line-scanning mode. (**D**) The ΔF/F0 images, obtained by averaging the
957 responses to odor stimuli over a duration of 5 seconds, corresponding to 15 frames,
958 were quantified. The plots of different compartments derived from the same sample are
959 interconnected with dashed lines. The bar graph illustrates the mean values. Asterisks
960 indicate significant differences. Dunn's multiple comparisons test for all pairwise
961 combinations, *$p < 0.05$, **$p < 0.01$, ***$p < 0.001$, ****$p < 0.0001$; $n = 10$. (E) The focal
962 plane of live imaging for compartments γ1-γ5 is presented (Upper panel). The ΔF/F0
963 images of averaged peak responses (10 frames, 5 s) of calcium and cAMP during the
964 presentations of MCH, OCT, ACV, and shock in compartments γ1-γ5 of the fly
965 expressing G-Flamp1 and jRGECO1b driven by the MB364B split Gal4 driver (lower
966 panels). (**F**) The focal plane of live imaging for the α3/α'3 compartments is presented.
967 Magnified images of averaged peak ΔF/F0 responses (10 frames, 5 s) of calcium and
968 cAMP in the α3 and α'3 compartments of the fly expressing G-Flamp1 and jRGECO1b
969 driven by the OK107-Gal4 driver. (**G**) The ΔF/F0 images, obtained by averaging the
970 responses to odor stimuli over a duration of 5 seconds, corresponding to 10 frames,
971 were quantified. The plots of different compartments derived from the same sample are

interconnected with dashed lines. The bar graph illustrates the mean values. Asterisks indicate significant differences. Dunn's multiple comparisons test for all pairwise combinations, *$p < 0.05$; $n = 10$.

Figure 2

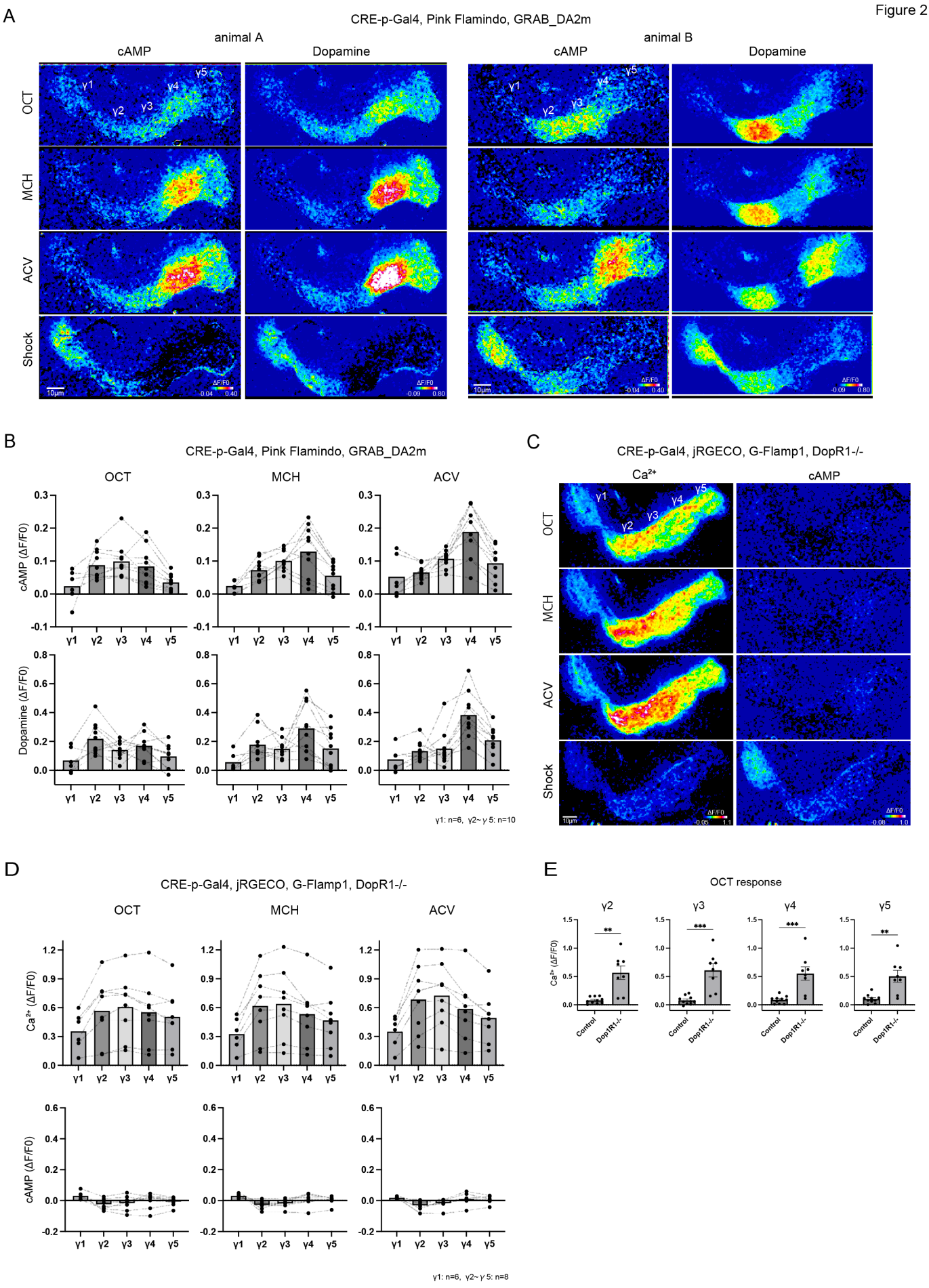
A
CRE-p-Gal4, Pink Flamindo, GRAB_DA2m
animal A
animal B
cAMP
Dopamine
OCT
MCH
ACV
Shock
γ1
γ2
γ3
γ4
γ5
10μm
ΔF/F0
B
CRE-p-Gal4, Pink Flamindo, GRAB_DA2m
OCT
MCH
ACV
cAMP (ΔF/F0)
Dopamine (ΔF/F0)
γ1: n=6, γ2~γ5: n=10
C
CRE-p-Gal4, jRGECO, G-Flamp1, DopR1-/-
Ca²⁺
cAMP
D
CRE-p-Gal4, jRGECO, G-Flamp1, DopR1-/-
Ca²⁺ (ΔF/F0)
cAMP (ΔF/F0)
γ1: n=6, γ2~γ5: n=8
E
OCT response
Control
DopR1-/-

991 **Figure 2.** Dopamine induces cAMP synthesis. (**A**) Two examples (animals A and B) of
992 ΔF/F0 images of averaged peak responses (10 frames, 3.3 s) of dopamine and cAMP
993 during the presentations of MCH, OCT, ACV, and shock in the γ1-γ5 compartments of
994 the fly expressing GRAB_DA2m and G-Flamp1 sensors driven by the γCRE-p-Gal4
995 driver. (**B**) The ΔF/F0 images, obtained by averaging the responses to odor stimuli,
996 were quantified. The plots of different compartments derived from the same sample are
997 interconnected with dashed lines. The bar graph illustrates the mean values. γ1: n =
998 6, γ2-γ5: n = 10. (**C**) Representative ΔF/F0 images of averaged peak responses (15
999 frames, 5 s) of calcium and cAMP during the presentations of MCH, OCT, ACV, and
1000 Shock in compartments γ1-5 expressing jRGECO1b and G-Flamp1 driven by the
1001 γCRE-p-Gal4 driver of the fly mutant for Dop1R1. (**D**) The ΔF/F0 images, obtained by
1002 averaging the responses to odor stimuli, were quantified. The plots of different
1003 compartments derived from the same sample are interconnected with dashed lines.
1004 The bar graph represents the mean values. γ1: n = 6, γ2-γ5: n = 8. (**E**) Comparison of
1005 the odor-evoked calcium responses in compartments γ2-γ5 between control and
1006 Dop1R1 mutant flies. Mann-Whitney U test, *$p < 0.05$, **$p < 0.01$, and ***$p < 0.001$;
1007 control: n = 10; Dop1R1 mutant: n = 9. The bar graph represents the mean values.
1008

Figure 3

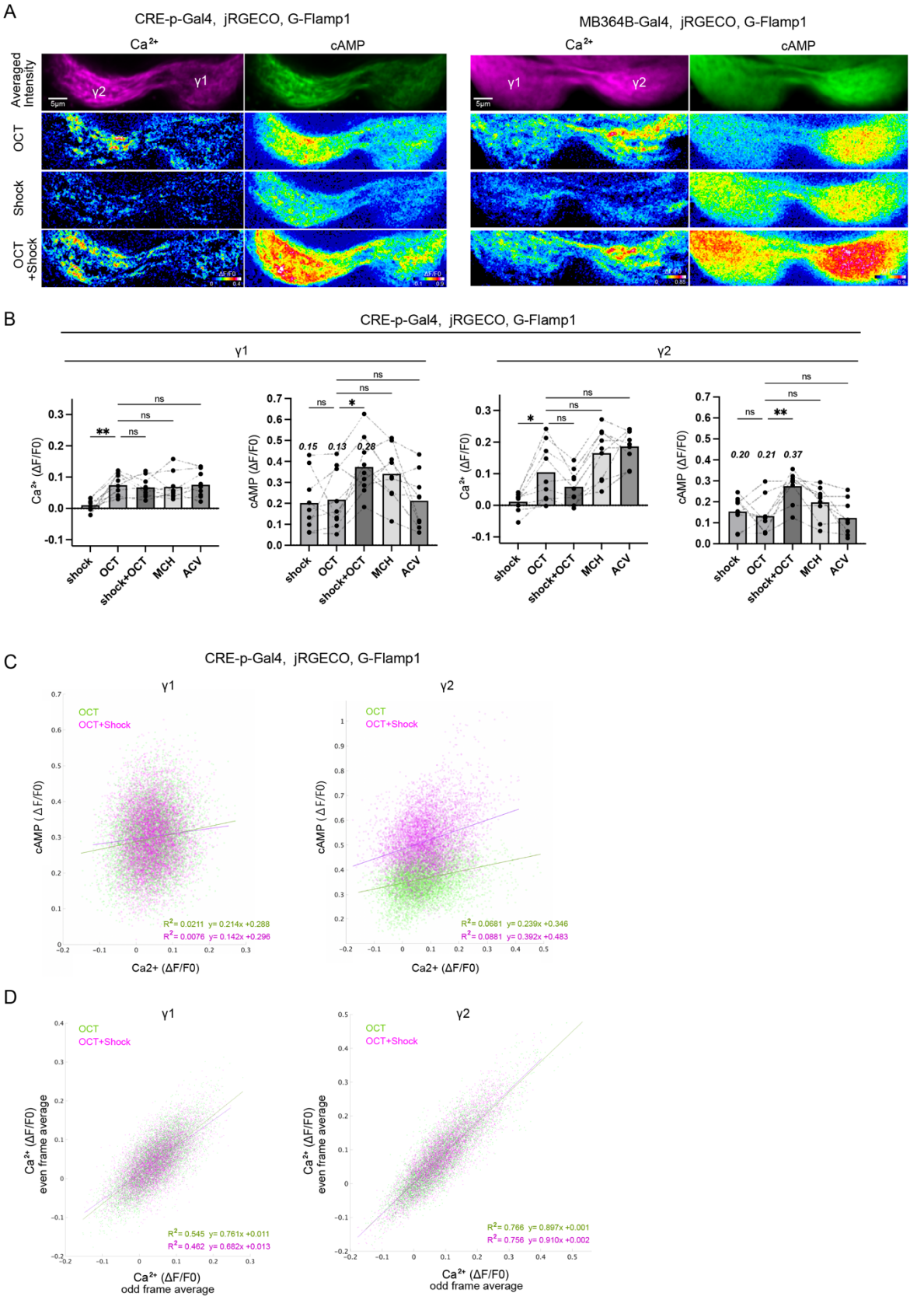
A
CRE-p-Gal4, jRGECO, G-Flamp1
MB364B-Gal4, jRGECO, G-Flamp1
Ca2+
cAMP
Averaged Intensity
OCT
Shock
OCT +Shock
γ1
γ2
5μm
B
CRE-p-Gal4, jRGECO, G-Flamp1
γ1
γ2
Ca2+ (ΔF/F0)
cAMP (ΔF/F0)
shock
OCT
shock+OCT
MCH
ACV
ns
*
**
0.15
0.13
0.28
0.20
0.21
0.37
C
CRE-p-Gal4, jRGECO, G-Flamp1
γ1
γ2
OCT
OCT+Shock
cAMP (ΔF/F0)
Ca2+ (ΔF/F0)
R2= 0.0211 y= 0.214x +0.288
R2= 0.0076 y= 0.142x +0.296
R2= 0.0681 y= 0.239x +0.346
R2= 0.0881 y= 0.392x +0.483
D
γ1
γ2
OCT
OCT+Shock
Ca2+ (ΔF/F0) even frame average
Ca2+ (ΔF/F0) odd frame average
R2= 0.545 y= 0.761x +0.011
R2= 0.462 y= 0.682x +0.013
R2= 0.766 y= 0.897x +0.001
R2= 0.756 y= 0.910x +0.002

1010 **Figure 3.** The cAMP levels during the pairing of olfactory stimuli with electric shock. (**A**)
1011 The top panels display the averaged representations of raw intensity values extracted
1012 from 80 frames, spanning a duration of 40 seconds including both stimulus and non-
1013 stimulus periods. The following three panels below present exemplary ΔF/F0 images of
1014 averaged peak responses (15 frames, 5 s) of calcium and cAMP during the
1015 presentation of OCT, Shock, and both in the γ1-γ2 compartments expressing
1016 jRGECO1b and G-Flamp1 driven by the γCRE-p (left) or MB364B GAL4 (right) driver.
1017 (**B**) The ΔF/F0 images, obtained by averaging the responses to stimuli of the fly
1018 expressing jRGECO1b and G-Flamp1 driven by the γCRE-p, were quantified. The plots
1019 of different stimuli derived from the same sample are interconnected with dashed lines.
1020 The bar graph illustrates the mean values. The Dunn's multiple comparisons test was
1021 conducted using OCT (CS+) stimulation as the control group to examine differences
1022 between the other stimulus groups, *$p < 0.05$, **$p < 0.01$; $n = 9$. (**C**) Scatter plots of
1023 ΔF/F0 values derived from representative averaged calcium and cAMP images of each
1024 γ compartment. These values are derived from the same dataset used in (**B**). The X-
1025 axis represents the ΔF/F0 of calcium, while the Y-axis represents the ΔF/F0 of cAMP.
1026 The individual points in the plot correspond to each pixel within the γ1 or γ2
1027 compartment in the averaged ΔF/F0 images, and linear regression lines are plotted.

OCT (CS only): green, and OCT + Shock (CS + US): magenta. (**D**) The X-axis and Y-axis represent the ΔF/F0 of calcium obtained by averaging odd frames and even frames, respectively, from the same calcium imaging data set used in (**C**). The individual points in the plot correspond to each pixel within the γ1 or γ2 compartment, and linear regression lines are plotted. OCT (CS only): green, and OCT + Shock (CS + US): magenta.

Figure 4

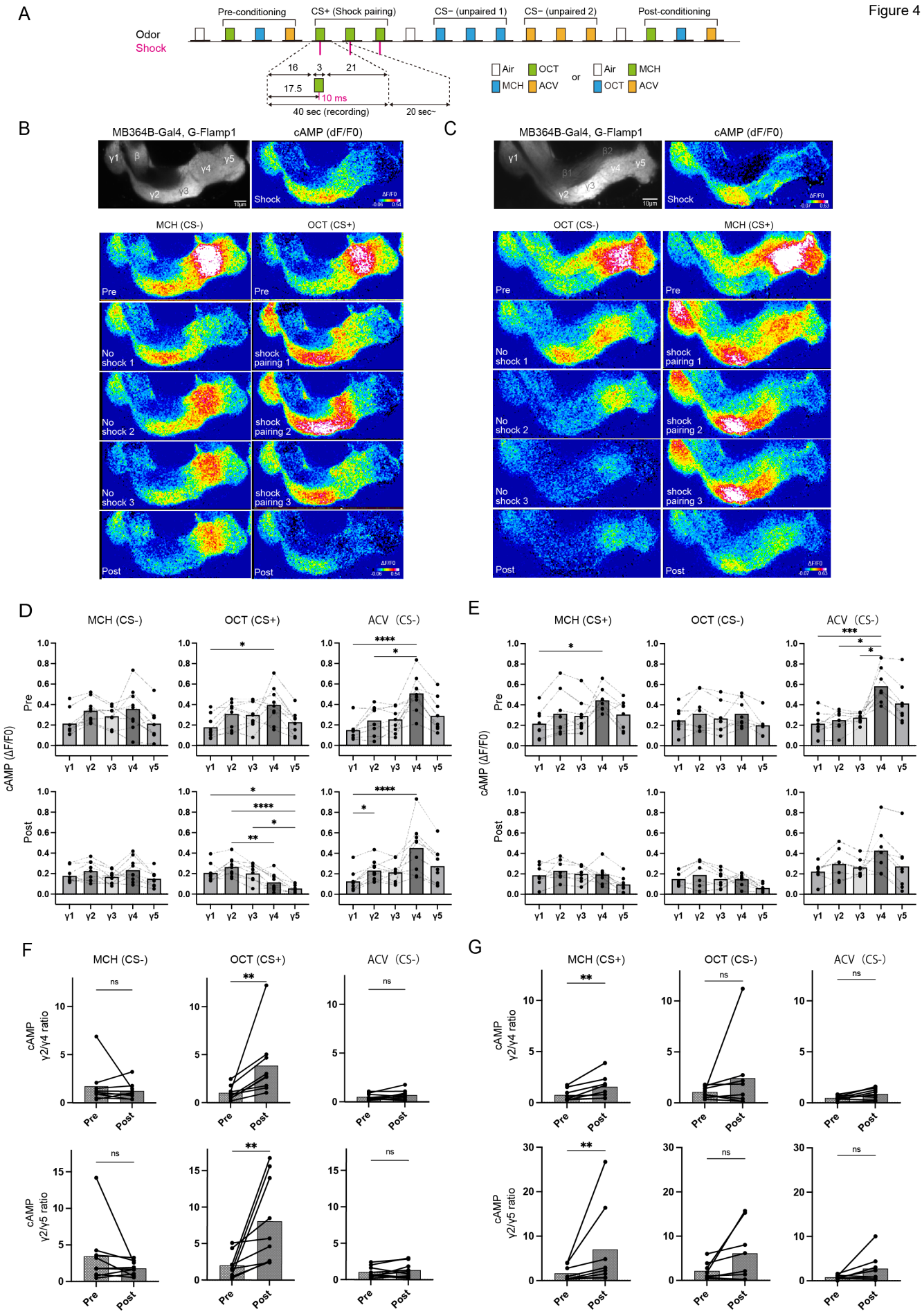
A
Pre-conditioning
CS+ (Shock pairing)
CS− (unpaired 1)
CS− (unpaired 2)
Post-conditioning
Odor
Shock
16
3
21
17.5
10 ms
40 sec (recording)
20 sec~
Air
OCT
MCH
ACV
or
Air
MCH
OCT
ACV
B
MB364B-Gal4, G-Flamp1
cAMP (dF/F0)
Shock
MCH (CS-)
OCT (CS+)
Pre
No shock 1
shock pairing 1
No shock 2
shock pairing 2
No shock 3
shock pairing 3
Post
C
MB364B-Gal4, G-Flamp1
cAMP (dF/F0)
Shock
OCT (CS-)
MCH (CS+)
Pre
No shock 1
shock pairing 1
No shock 2
shock pairing 2
No shock 3
shock pairing 3
Post
D
MCH (CS-)
OCT (CS+)
ACV (CS-)
cAMP (ΔF/F0)
Pre
Post
E
MCH (CS+)
OCT (CS-)
ACV (CS-)
cAMP (ΔF/F0)
Pre
Post
F
MCH (CS-)
OCT (CS+)
ACV (CS-)
cAMP γ2/γ4 ratio
cAMP γ2/γ5 ratio
ns
Pre
Post
G
MCH (CS+)
OCT (CS-)
ACV (CS-)
cAMP γ2/γ4 ratio
cAMP γ2/γ5 ratio
ns
Pre
Post

1047 **Figure 4.** The plastic changes of the cAMP code associated with aversive conditioning.
1048 (**A**) Schematic representation of conditioning procedure. Sixteen seconds after the start
1049 of the recording, a 3 second odor stimulus was presented to the fly. Following a delay
1050 of 1.5 seconds from the onset of the odor presentation, an electric shock of 60 volts
1051 was administered to the fly for a duration of 10 milliseconds. In a series of experiments,
1052 OCT was paired with electric shock, while MCH and ACV were not (**B**). In another set
1053 of experiments, MCH was paired with electric shock, while OCT and ACV were not (**C**).
1054 (**B**, **C**) All the cAMP images in compartments γ1-5 were captured from the flies
1055 expressing G-Flamp1 and jRGECO1b under the control of the MB364B driver. An
1056 averaged raw intensity image of cAMP derived from 80 frames acquired during air
1057 presentation for 40 s (upper left), and the ΔF/F0 image obtained by averaging the
1058 responses (5 s, 10 frames) to electric shock (upper right) are shown. The images
1059 displayed below depict the ΔF/F0 images obtained by averaging the neural responses
1060 (5 s, 10 frames) to OCT (as CS+) during the pre-conditioning, first, second, and third
1061 pairings, as well as post-conditioning. Additionally, the images illustrate the neural
1062 responses to MCH (as CS-) during the same experimental procedure, but without
1063 electric shock (**B**). Similarly, the corresponding images obtained when MCH was
1064 presented as the CS+ and OCT as the CS- (**C**). (**D**, **E**) The ΔF/F0 images, obtained by

1065 averaging the pre- and post-conditioning-responses to odors, were quantified. The
1066 identical datasets employed in (**B**) and (**C**) were utilized for (**D**) and (**E**), respectively.
1067 Additionally, the responses to ACV were included as the second CS-. The plots of
1068 different compartments derived from the same sample are interconnected with dashed
1069 lines. The bar graph illustrates the mean values. Asterisks indicate significant
1070 differences. Dunn's multiple comparisons test for all pairwise combinations, *$p < 0.05$,
1071 **$p < 0.01$, ***$p < 0.001$, ****$p < 0.0001$; n = 9 (**D**) and 8 (**E**). (**F**, **G**) For each odor, the
1072 ratio of cAMP levels in the γ2 compartment to those in the γ4 or γ5 compartment was
1073 determined, and these ratios are referred to as the γ2/4 cAMP ratio or the γ2/5 cAMP
1074 ratio. The ratios obtained before and after the conditioning phase are then compared.
1075 The same datasets used in (**D**) and (**E**) were utilized for (**F**) and (**G**), respectively.
1076 Wilcoxon signed rank test, **$p < 0.01$; n=9 (**F**), 8 (**G**).
1077
1078
1079
1080
1081

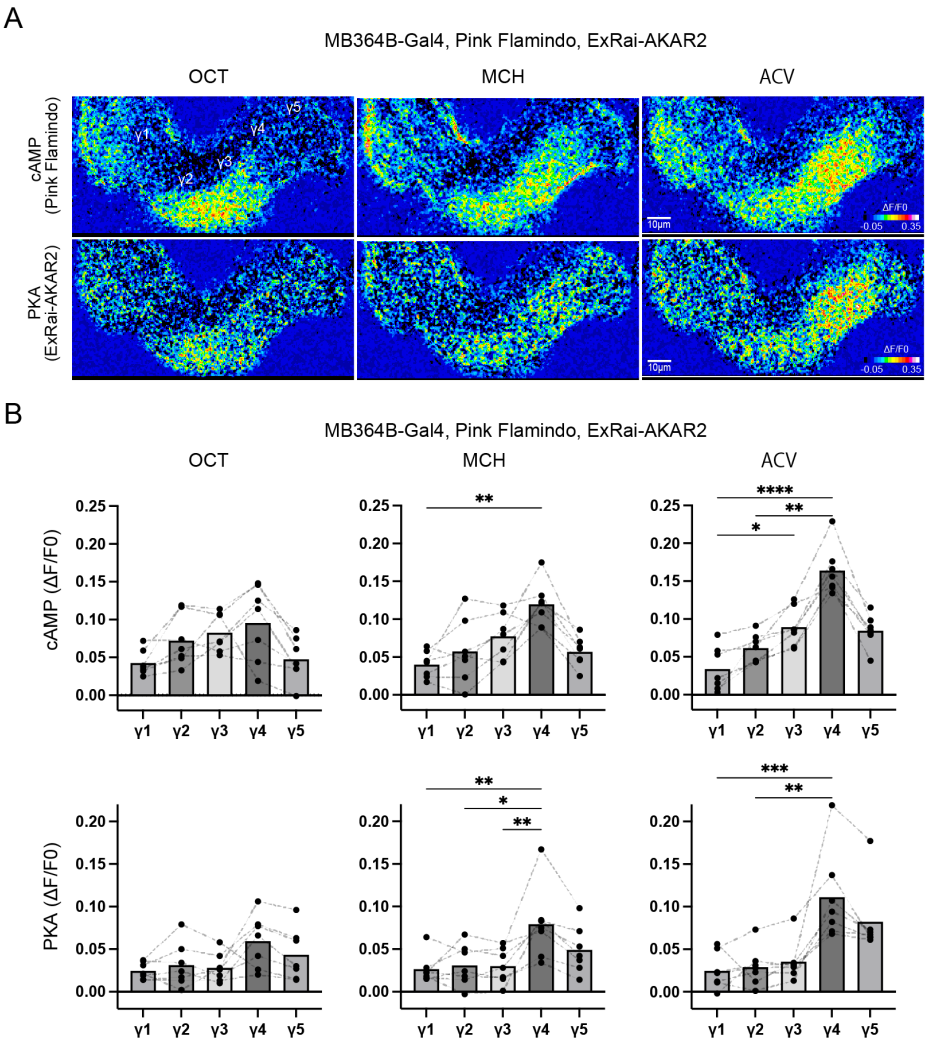

Figure 5. The protein kinase A (PKA) activities coincide with the presence of cAMP. (**A**) The ΔF/F0 images obtained by averaging the responses (5 s, 10 frames) in γ1-γ5 compartments during OCT, MCH or ACV presentation to the fly expressing Pink Flamindo for cAMP detection and ExRai-AKAR2 for PKA activity detection under the control of MB364B driver are shown. (**B**) Quantification of the averaged peak ΔF/F0

1087 images of cAMP (upper panels) and PKA activity (lower panels). The plots of different

1088 compartments derived from the same sample are connected by dashed lines. The bar

1089 graph represents the mean values. Significant differences are denoted with asterisks.

1090 Dunn's multiple comparisons test for all pairwise combinations, *$p < 0.05$, **$p < 0.01$,

1091 ***$p < 0.001$; $n = 7$.

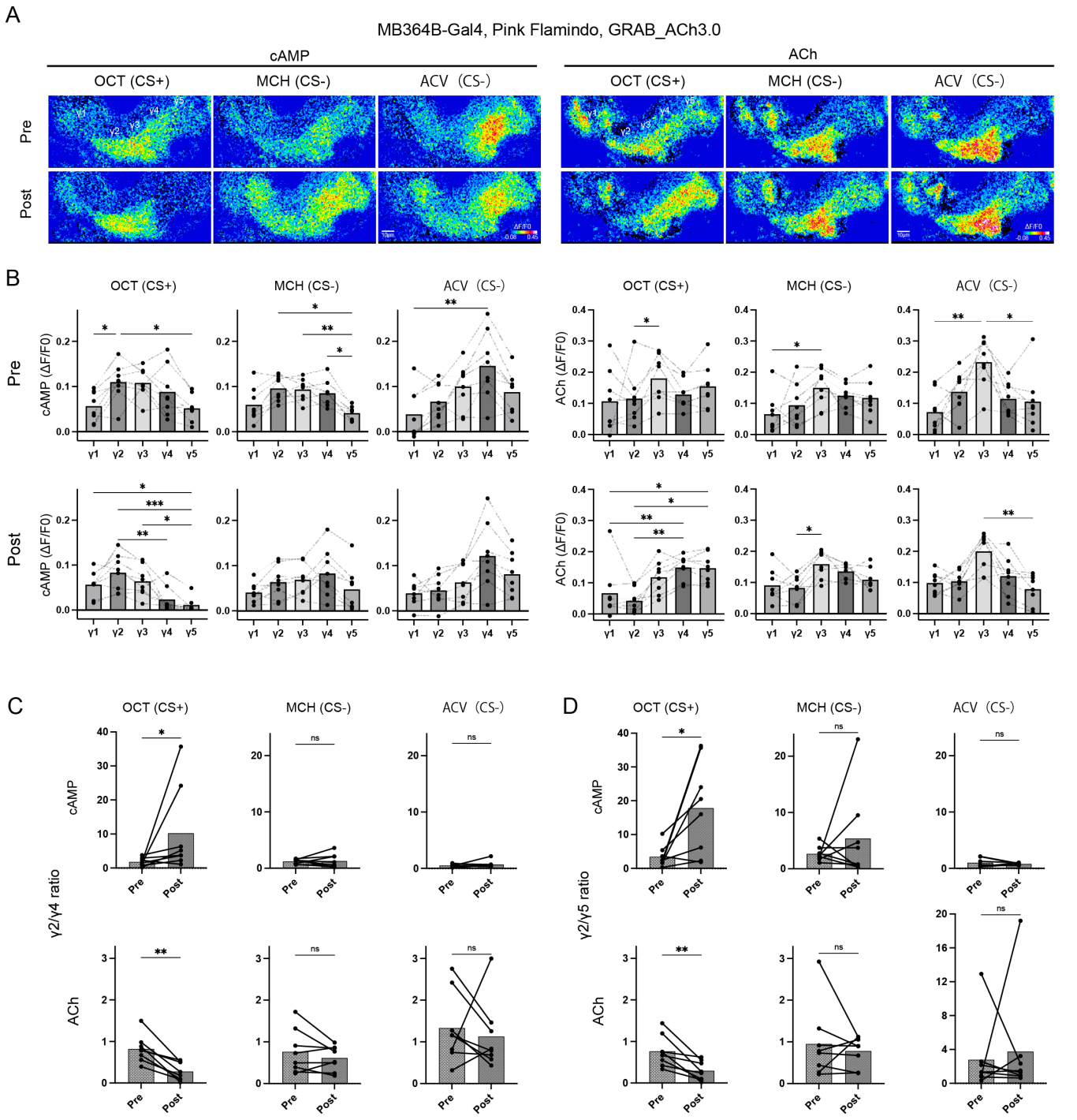

Figure 6. Plasticity in the release of acetylcholine (ACh) from KCs associated with the process of aversive conditioning. Flies expressing Pink Flamindo and GRAB_ACh under the control of the MB364B-Gal4 driver were subjected to aversive conditioning,

following the procedure outlined in Figure 4. (**A**) The ΔF/F0 images, depicting the averaged peak responses (10 frames for 5 s) of cAMP (left) and ACh (right) in γ1-γ5 compartments, were captured during the presentations of OCT (CS+), MCH (CS-), and ACV (CS-) before (Pre) and after (Post) conditioning. (**B**) The ΔF/F0 images of cAMP (left) and ACh (right) obtained by averaging the pre- and post-conditioning responses to odors were quantified. The plots of different compartments derived from the same sample are interconnected with dashed lines. The bar graph illustrates the mean values. Asterisks indicate significant differences. Dunn's multiple comparisons test for all pairwise combinations, *$p < 0.05$, **$p < 0.01$, ***$p < 0.001$; $n = 8$. (**C**) Comparisons of the γ2/4 cAMP ratios before and after the conditioning phase for each odor (upper panel). Similarly, the γ2/4 ACh ratios before and after the conditioning phase are compared (lower panel). (**D**) Comparisons of the γ2/5 cAMP ratios before and after the conditioning phase for each odor (upper panel). The γ2/5 ACh ratios before and after the conditioning phase are compared (lower panel). (**C**, **D**) Wilcoxon signed rank test, *$p < 0.05$, **$p < 0.01$; $n=8$.

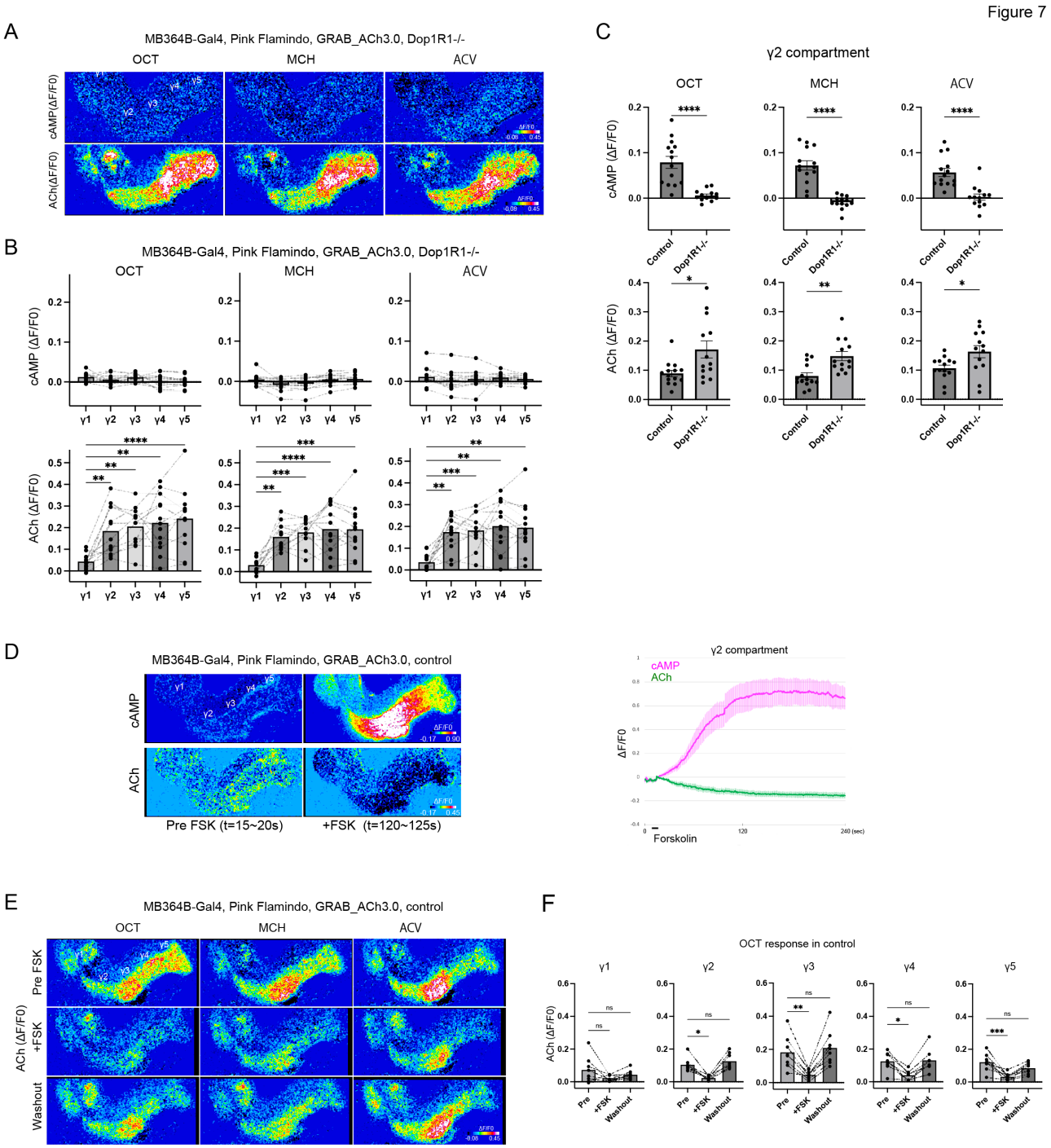

Figure 7. (**A**) Exemplary ΔF/F0 images of averaged peak responses (10 frames for 5 s) of cAMP and ACh during the presentations of MCH, OCT, and ACV in the γ1-γ5 compartments of the Dop1R1 mutant flies expressing Pink Flamindo and GRAB_ACh

1113 driven by the MB364B-Gal4 driver. (**B**) The ΔF/F0 images of cAMP and Ach, obtained
1114 by averaging the odor responses of the flies described in (A), were quantified. The
1115 plots of different compartments derived from the same sample are interconnected with
1116 dashed lines. The bar graph illustrates the mean values. Asterisks indicate significant
1117 differences. Dunn's multiple comparisons test for all pairwise combinations, *p < 0.05,
1118 **p < 0.01, ***p < 0.001, ****p < 0.0001; n = 13. (**C**) The ΔF/F0 images of cAMP and
1119 ACh, obtained by averaging the responses to odors in the γ2 compartment of the
1120 Dop1R1 mutant described in (A), were quantified, and compared with those of the
1121 genetic control (harboring the wild-type Dop1R1). Mann-Whitney U test, *p < 0.05, **p
1122 < 0.01, ****p < 0.0001; n= 14 (control) and 13 (Dop1R1). (**D**) The ΔF/F0 images of
1123 cAMP and ACh were obtained by averaging the responses immediately after (pre FSK)
1124 and 2 minutes after (+ FSK) switching from standard saline to saline containing 100 μM
1125 Forskolin (left). These and the following measurements were obtained in flies
1126 expressing Pink Flamindo and $GRAB_{ACh}$ under the control of the MB364B-Gal4 driver.
1127 The time series traces of cAMP (magenta) and ACh (green) are shown (right),
1128 illustrating the changes in their levels after the switch to saline containing 100 μM
1129 Forskolin. The line and shading represent the mean ± SEM. n = 8. (**E**) ΔF/F0 images of
1130 averaged peak responses (10 frames for 5 s) of ACh during the presentation of OCT,

MCH, or ACV. These measurements were obtained under three conditions: standard saline (Pre FSK), four minutes after switching to saline containing 100 μM Forskolin (+ FSK), and after returning to standard saline (Washout). (**F**) The averaged peak ΔF/F0 responses of ACh to OCT in pre-Forskolin, +Forskolin, and Washout conditions, as depicted in (**E**), were quantified for each compartment. The plots of different conditions derived from the same sample are interconnected with dashed lines. The bar graph illustrates the mean values. Asterisks indicate significant differences. Dunn's multiple comparisons test, *$p < 0.05$, **$p < 0.01$, ***$p < 0.001$; $n = 8$.

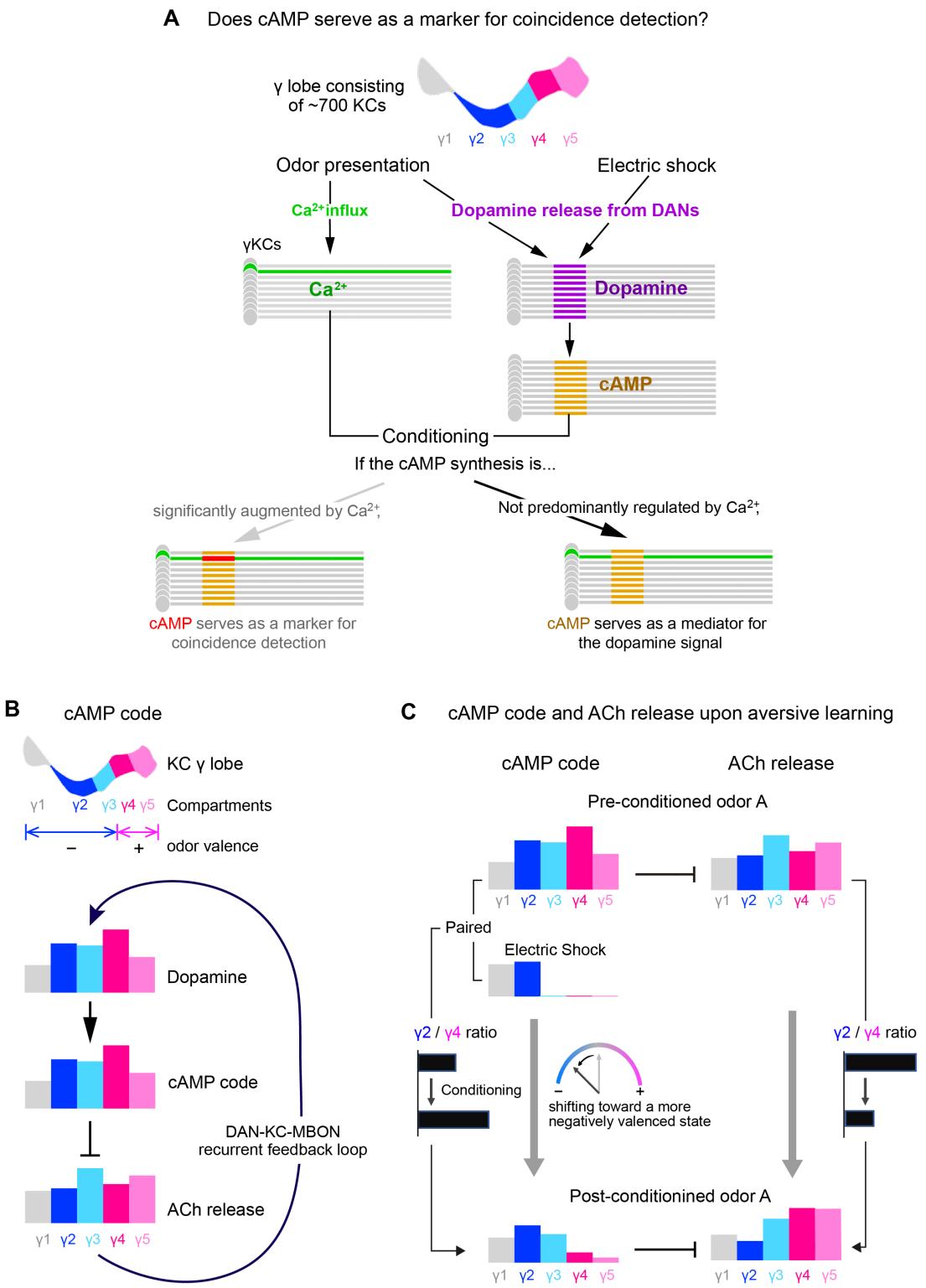

Figure 8. The role of the cAMP signal in aversive olfactory memory. (**A**) Does cAMP serve as a marker for coincidence detection? The γ lobe comprises approximately 700

1151 Kenyon cells (KCs) and is partitioned into five compartments, and each receives its
1152 own distinct dopaminergic innervation. Each olfactory stimulus elicits calcium transients
1153 in a unique subset of approximately 20% of KCs and activates a specific subset of the
1154 dopaminergic neurons. Consequently, KCs receive compartment-specific dopamine
1155 signals along the entire length of the lobe, exhibiting distinct characteristics for each
1156 odor. The release of dopamine occurs through volume transmission, leading to its
1157 detection in a population of axons that spans nearly the entire breadth of the lobe. This
1158 detection roughly coincides with the presence of cAMP. If the synthesis of cAMP is
1159 significantly enhanced by calcium, then the axons with high calcium signals exhibit
1160 elevated cAMP synthesis. Conversely, if calcium does not predominantly regulate
1161 cAMP synthesis, then the axons activated by olfactory stimuli are not distinguished by
1162 their cAMP levels. Our findings corroborate the latter hypothesis and indicate that
1163 cAMP serves as a mediator of the dopamine signal. (B) cAMP code. cAMP levels in
1164 each compartment depend on receiving dopamine conveying negative valence to the
1165 γ1-3 compartments and positive valence to the γ4-5 compartments. The global
1166 equilibrium of cAMP levels throughout the γ lobe could yield a comprehensive depiction
1167 of the integrated valence, which can be portrayed as a two-dimensional image of cAMP
1168 levels and designated as the cAMP code. KCs exert regulatory control over the

functions of their downstream targets; namely, the mushroom body output neurons (MBONs), through the release of acetylcholine (ACh). cAMP serves as a negative regulator of ACh release. In turn, the MBONs reciprocally modulate dopaminergic activities, thereby establishing a complex DAN-KC-MBON recurrent feedback loop (Adel and Griffith, 2021). (**C**) cAMP code and ACh release upon aversive learning. When an odor A is associated with electric shock, the cAMP code of the odor A is integrated with the cAMP code of the electric shock. It can be inferred that the relative cAMP levels of the γ2 (corresponding to negative valence) to the γ4 or γ5 (corresponding to positive valence) compartment, the γ2/4 or γ2/5 cAMP ratio, may have the potential to serve as a quantitative measure for evaluating the valence of an olfactory stimulus for an individual. As the conditioning process advances, the integrated cAMP code tilts towards a negative valence, culminating in the formation of an aversively acquired cAMP code for the odor that persists even after conditioning. The release of ACh from KCs is attenuated by cAMP, consequently establishing a roughly antithetical relationship between the ACh release profile and the cAMP code profile across compartments.